Cell Reports

Article

The AP1 Transcription Factor Fosl2 Promotes Systemic Autoimmunity and Inflammation by Repressing Treg Development

Graphical Abstract

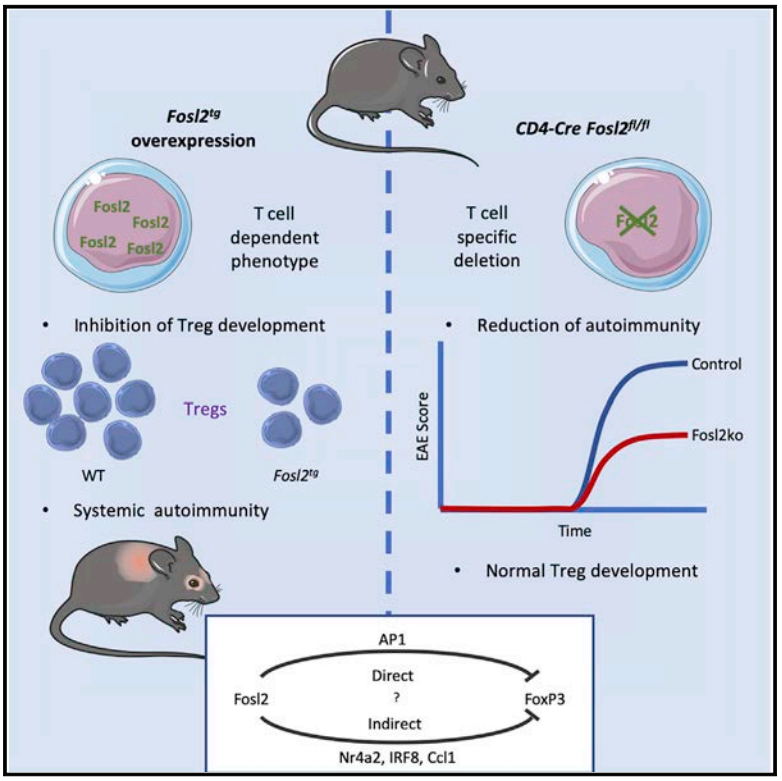

Highlights

- Mice overexpressing Fosl2 develop autoimmune T cell-mediated systemic inflammation
- Elevated Fosl2 in T cells represses thymic Treg development
- T cell-specific Fosl2 deletion reduces disease severity in EAE

Authors

Florian Renoux, Mara Stellato, Claudia Haftmann, ..., Gabriela Kania, Onur Boyman, Oliver Distler

Correspondence

oliver.distler@usz.ch

In Brief

Renoux et al. investigate the role of the AP1 member Fosl2 in autoimmunity. They show that Fosl2 overexpression induces T cell-mediated systemic inflammation in transgenic mice, while Fosl2 deletion in T cells protects against induced autoimmunity. Furthermore, they suggest that Fosl2 is implicated in Treg development in the thymus.

Renoux et al., 2020, Cell Reports *31*, 107826
June 30, 2020 © 2020 The Authors.
https://doi.org/10.1016/j.celrep.2020.107826

CellPress

Cell Reports

CellPress
OPEN ACCESS

Article

The AP1 Transcription Factor Fosl2 Promotes Systemic Autoimmunity and Inflammation by Repressing Treg Development

Florian Renoux,[1] Mara Stellato,[1] Claudia Haftmann,[2] Alexander Vogetseder,[3] Riyun Huang,[4] Arun Subramaniam,[4] Mike O. Becker,[1] Przemyslaw Blyszczuk,[1,5] Burkhard Becher,[2] Jörg H.W. Distler,[6] Gabriela Kania,[1] Onur Boyman,[7,8] and Oliver Distler[1,8,9,*]

[1]Center of Experimental Rheumatology, Department of Rheumatology, University Hospital Zurich, Zurich, Switzerland
[2]Institute of Experimental Immunology, University of Zurich, Zurich, Switzerland
[3]Department of Pathology, Luzerner Kantonspital, Lucerne, Switzerland
[4]Sanofi, Immunology and Inflammation Research TA, Cambridge, MA 02139, USA
[5]Department of Clinical Immunology, Jagiellonian University Medical College, Cracow, Poland
[6]Department of Internal Medicine 3, University of Erlangen-Nuremberg, Erlangen, Germany
[7]Department of Immunology, University Hospital Zurich, Zurich, Switzerland
[8]Faculty of Medicine, University of Zurich, Zurich, Switzerland
[9]Lead Contact
*Correspondence: oliver.distler@usz.ch
https://doi.org/10.1016/j.celrep.2020.107826

SUMMARY

Regulatory T cells (Tregs) represent a major population in the control of immune homeostasis and autoimmunity. Here we show that Fos-like 2 (Fosl2), a TCR-induced AP1 transcription factor, represses Treg development and controls autoimmunity. Mice overexpressing Fosl2 (*Fosl2*^{tg}) indeed show a systemic inflammatory phenotype, with immune infiltrates in multiple organs. This phenotype is absent in *Fosl2*^{tg} × *Rag2*$^{-/-}$ mice lacking T and B cells, and Fosl2 induces T cell-intrinsic reduction of Treg development that is responsible for the inflammatory phenotype. *Fosl2*^{tg} T cells can transfer inflammation, which is suppressed by the co-delivery of Tregs, while Fosl2 deficiency in T cells reduces the severity of autoimmunity in the EAE model. We find that Fosl2 could affect expression of FoxP3 and other Treg development genes. Our data highlight the importance of AP1 transcription factors, in particular Fosl2, during T cell development to determine Treg differentiation and control autoimmunity.

INTRODUCTION

CD4^{+} T cells can differentiate into various subsets of helper cells, which enables the adaptation of the immune response to different pathogens. Regulatory T cells (Tregs), on the other hand, are a population of T cells that are able to control other immune cell types. Forkhead box protein P3 (FoxP3) was identified as the key transcription factor for Treg identification and function (Bennett et al., 2001; Chatila et al., 2000). The main source of Tregs is the thymus, where CD4 single-positive (SP) thymocytes acquire a Treg phenotype directly from the developmental stage (Owen et al., 2019). These thymic-derived Tregs are called natural Tregs (nTregs) or thymic Tregs (tTregs) and rely mostly on T cell receptor (TCR) and IL-2 signals. Mature T cells in the periphery can also be induced to express FoxP3 and to acquire suppressive capacities when activated in the presence of IL-2 and TGF-β, giving rise to induced Tregs (iTregs), also called peripheral Tregs (pTregs) (Chen et al., 2003).

Tregs are central in the control of immune response. Evidences in humans was provided by an IPEX (immune dysregulation, polyendocrinopathy, enteropathy, X-linked syndrome) patient with a loss-of-function mutation in FoxP3, which clearly demonstrated the requirement for Tregs to maintain immune tolerance and prevent autoimmunity (Bennett et al., 2001; Brunkow et al., 2001). Studies have also suggested that abnormalities in Treg numbers, frequencies, and suppressive function could be involved in the pathomechanisms of multiple autoimmune diseases (Grant et al., 2015). On the other hand, Tregs were also shown to suppress antitumor responses, worsening disease outcome (Facciabene et al., 2012). Although recent data have provided good knowledge of the identity and function of Tregs, how the fate decision and differentiation of these cells are controlled is still only partly understood.

Fos-like 2 (Fosl2; also called Fos-related antigen-2 [Fra-2]) is a member of the Fos family and belongs to the AP1 transcription complex. AP1 is a complex network of heterodimers formed by proteins of the Jun, Fos, ATF, and MAF families, comprising more than 20 proteins in total. These AP1 proteins have a basic DNA-binding domain that is active only when the protein forms a dimer through its leucine zipper region. With the exception of Jun proteins that can form homodimers, other AP1 proteins always function in tandem with another AP1 protein in a heterodimer

This is an open access article under the CC BY-NC-ND license (http://creativecommons.org/licenses/by-nc-nd/4.0/).

(Hess et al., 2004). So far, Fosl2 interactions with Jun, JunB, JunD, and ATF7 have been confirmed (Mathas et al., 2009; Mazur et al., 2015; Bozec et al., 2013). Of note, these Jun proteins can themselves interact with other Fos or ATF proteins, creating a vast network of dimers exerting both redundant and unique functions (Hess et al., 2004). This mode of action has limited our understanding of individual AP1 protein functions, and AP1 is often referred to as one transcription complex irrespective of the proteins involved. So far, Fosl2 has been found to control bone formation (Bozec et al., 2010), promote fibrosis through fibroblast activation (Eferl et al., 2008), and participate in the control of B cell development (Ubieta et al., 2017). However, Fosl2 was initially thought to play a minimal role in T cells, as *Fosl2*$^{fl/fl}$ CD4-cre^{+} mice had no overt T cell phenotype and displayed only abnormal invariant natural killer T (iNKT) cells (Lawson et al., 2009). More recently, bioinformatic approaches using multiple datasets predicted a role for Fosl2 in controlling Th17 plasticity (Ciofani et al., 2012). Interestingly, several genome-wide association studies (GWASs) also reported associations of single-nucleotide polymorphisms (SNPs) within the promoter of Fosl2 with risk for Crohn's disease, ulcerative colitis, asthma, hay fever, and eczema (Jostins et al., 2012; Liu et al., 2015; Ye and McGovern, 2016; Ferreira et al., 2019), suggesting a possible role for Fosl2 in the control of inflammatory diseases.

AP1 members are known to contribute to Treg biology. Several binding sites have been found in the promoter and enhancer of FoxP3, and Jun and Fos in particular have been suggested to promote FoxP3 expression (Mantel et al., 2006; Bao et al., 2016). JunB was also identified to promote effector Treg homeostasis and suppressive function (Koizumi et al., 2018). In opposition, Batf3 was shown to repress Treg differentiation in the periphery, highlighting the diverse contributions of AP1 to Treg biology (Lee et al., 2017). So far the contribution of Fosl2 to AP1 function in T cells and in the control of inflammation and autoimmunity remains unknown.

RESULTS

Fosl2^{tg} Mice Develop a Multi-organ Inflammatory Phenotype

To explore the function of Fosl2, we analyzed the effects of both Fosl2 deficiency and Fosl2 overexpression. We generated a Fosl2 transgenic mouse strain (*Fosl2*^{tg}) in which the murine Fosl2 gene was randomly inserted under the control of the major histocompatibility complex class I (MHCI) promotor H2Kb (Figure S1A), using a similar strategy as previously described (Eferl et al., 2008). To obtain Fosl2-deficient T cells, we used *Fosl2*$^{fl/fl}$ and CD4-cre mice (Eferl et al., 2007) (Figure S1B). Successful deletion and overexpression of Fosl2 were confirmed on mRNA and protein levels in T cells from *Fosl2*$^{fl/fl}$CD4-cre^{+} and *Fosl2*^{tg} mice (Figures S1C and S1D).

We observed a spontaneous phenotype in *Fosl2*^{tg} mice. All *Fosl2*^{tg} mice developed dermatitis around the eyes, evidenced by extensive swelling and fur loss (Figures 1A and S2A). Interestingly, there was a difference in the onset of dermatitis development between males and females, with skin lesions developing at a median age of 13 weeks for females and 17.5 weeks for males. Dermatitis also affected the back and tail skin in certain mice but did not involve paws or ears. Histological analysis of affected skin revealed multifocal ulcerating inflammation with partial acanthosis and hyperkeratosis/hyperparakeratosis. Leukocyte infiltrates were present in the subcutaneous layer, dermis, and epidermis (Figure 1B).

Upon dissection, macroscopic examination of the mice also showed enlarged thymus, salivary glands, spleen, lungs, liver, and duodenum. Lungs and thymus were the most commonly affected organs, whereas other organs were differently affected between animals. As for skin, females had a more severe organ phenotype, with higher increases in spleen and liver weight than in males (Figure S1E).

Histological analysis of these organs revealed that inflammatory infiltrates were present in the lungs, thymus, salivary glands, pancreas, liver, and duodenum (Figures 1C and 1D; Figure S2B). In the lungs, there were perivascular and peribronchial leukocyte infiltrates, as evidenced by CD45 staining. There were also signs of interstitial pneumonitis with eosinophilic foamy macrophages and eosinophilic crystals (Figure 1C; Figure S2E). Transgenic mice displayed hypertrophy of thymus and salivary glands with inflammation (Figure S2B). Pancreas and liver showed diverse degrees of inflammation depending on the animals analyzed (Figure S2B).

Given the inflammation in multiple organs, we decided to analyze serum cytokines. Levels of 20 cytokines and chemokines were quantified in 12 wild-type (WT) and 12 *Fosl2*^{tg} mice at 17 weeks of age by multiplex analysis. Among these cytokines, we observed significant increases in TNF-α and IL-1β, confirming the strong inflammation present in *Fosl2*^{tg} mice (Figure 1E). Interestingly, levels of IL-5 were strongly increased, which correlated with the eosinophilia observed in several organs, especially the lungs. There were also smaller but significant increases in IL-6, IL-9, IL-10, and CCL-2 (Figure 1E).

Serum levels of total IgG were decreased in the serum of *Fosl2*^{tg} mice. In line with the presence of eosinophilia and elevated IL-5 levels in *Fosl2*^{tg} mice, we observed a significant increase in IgE levels (Figure S2D).

Rag2-Dependent Immune Cells Drive Pathology in *Fosl2*^{tg} Mice

Altogether, our observation showed a strong systemic inflammatory phenotype in *Fosl2*^{tg} mice. We thus investigated whether this phenotype resulted from a dysregulation of the adaptive immune system. To address this point, we crossed *Fosl2*^{tg} mice with *Rag2*$^{-/-}$ mice lacking B and T cells. Interestingly, none of the *Fosl2*^{tg}*Rag2*$^{-/-}$ mice developed dermatitis, even at the ages of 16 weeks for females and 22 weeks for males (Figures 1F and S3A), whereas all *Fosl2*^{tg} mice of these ages had to be euthanized because of the severity of dermatitis. *Fosl2*^{tg}*Rag2*$^{-/-}$ mice also did not show any signs of inflammation in other organs (lungs, salivary glands), indicating that the systemic inflammation observed in *Fosl2*^{tg} mice is dependent on adaptive immunity (Figures 1G, 1H, S3B, and S3C).

The absence of inflammation in *Rag2*$^{-/-}$*Fosl2*^{tg} mice pointed to the involvement of T cells. We thus analyzed the T cell compartment of *Fosl2*^{tg} mice (gating strategy in Figure S4). In 7-week-old mice, before the appearance of inflammation,

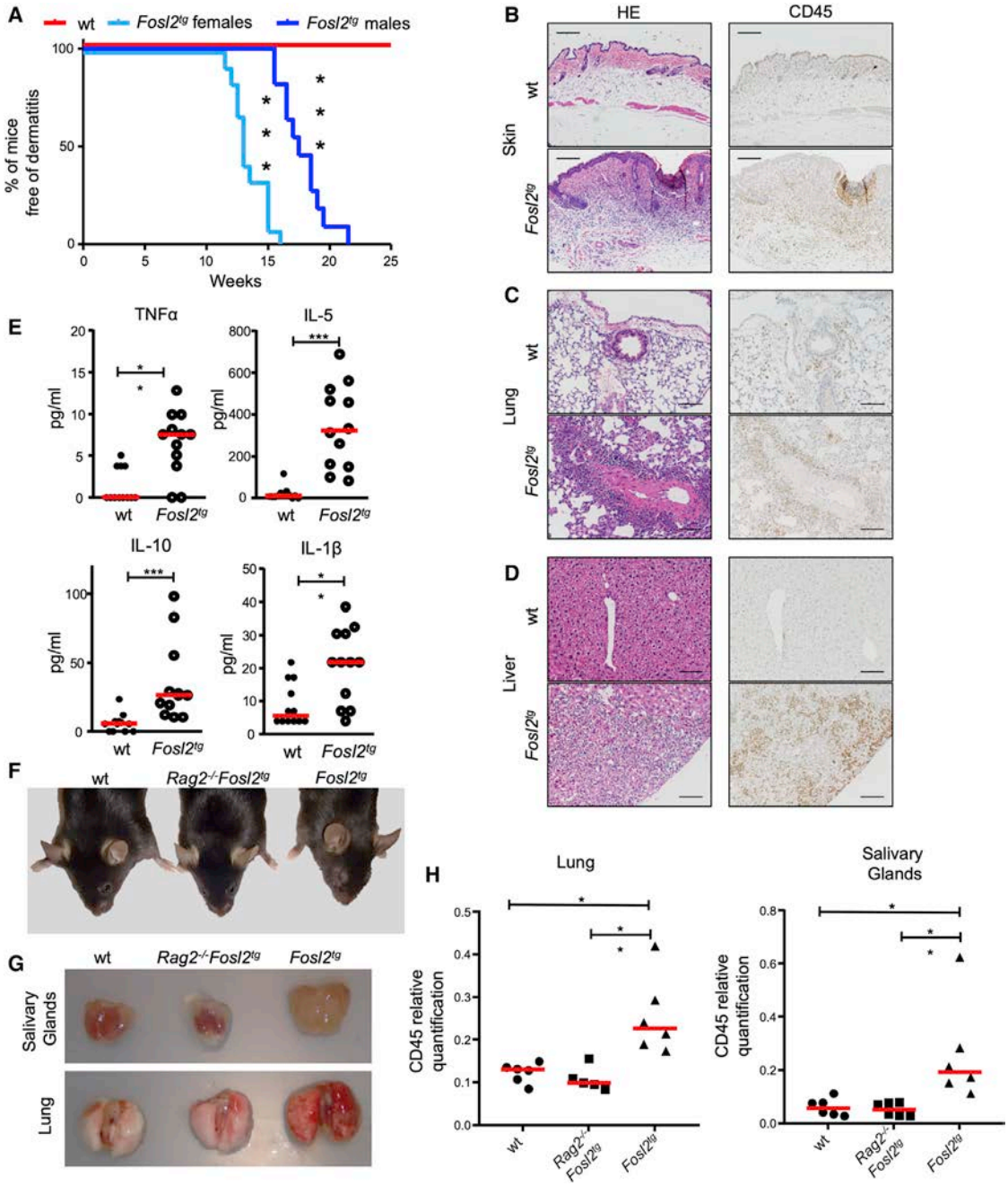

Figure 1. Fosl2^{tg} Mice Develop Systemic Inflammation

(A) Percentage of mice without skin lesions at different ages in weeks, for WT mice (females) and either *Fosl2^{tg}* males or females (n = 10–12 each).

(B–D) Representative pictures of paraffin-embedded skin (B), lung (C), and liver (D) sections with hematoxylin and eosin (left) and CD45 (right) staining from WT or *Fosl2^{tg}* mice (females, 16 weeks). Scale bars, 200 μm. (E) Multiplex analysis of cytokine levels in the serum of 17-week-old mice (males and females, n = 12).

(F) Representative picture of WT, *Fosl2^{tg}*, and *Rag2$^{-/-}$Fosl2^{tg}* mice showing skin lesions around the eyes only in the *Fosl2^{tg}* mouse.

(G) Representative pictures of submandibular salivary glands and lungs of WT, *Fosl2^{tg}*, and *Rag2$^{-/-}$Fosl2^{tg}* mice showing enlargement (salivary gland) and macroscopic lesions (lung) only in organs from *Fosl2^{tg}* mice.

(H) Relative quantification of CD45 staining. Number of CD45-positive pixels was quantified in the entire sections and normalized to nuclei staining.

*p < 0.05, **p < 0.01, and ***p < 0.001, Mantel-Cox test (A), Mann-Whitney test, two-tailed (E), and Kruskal-Wallis test with Dunn's multiple testing (H).

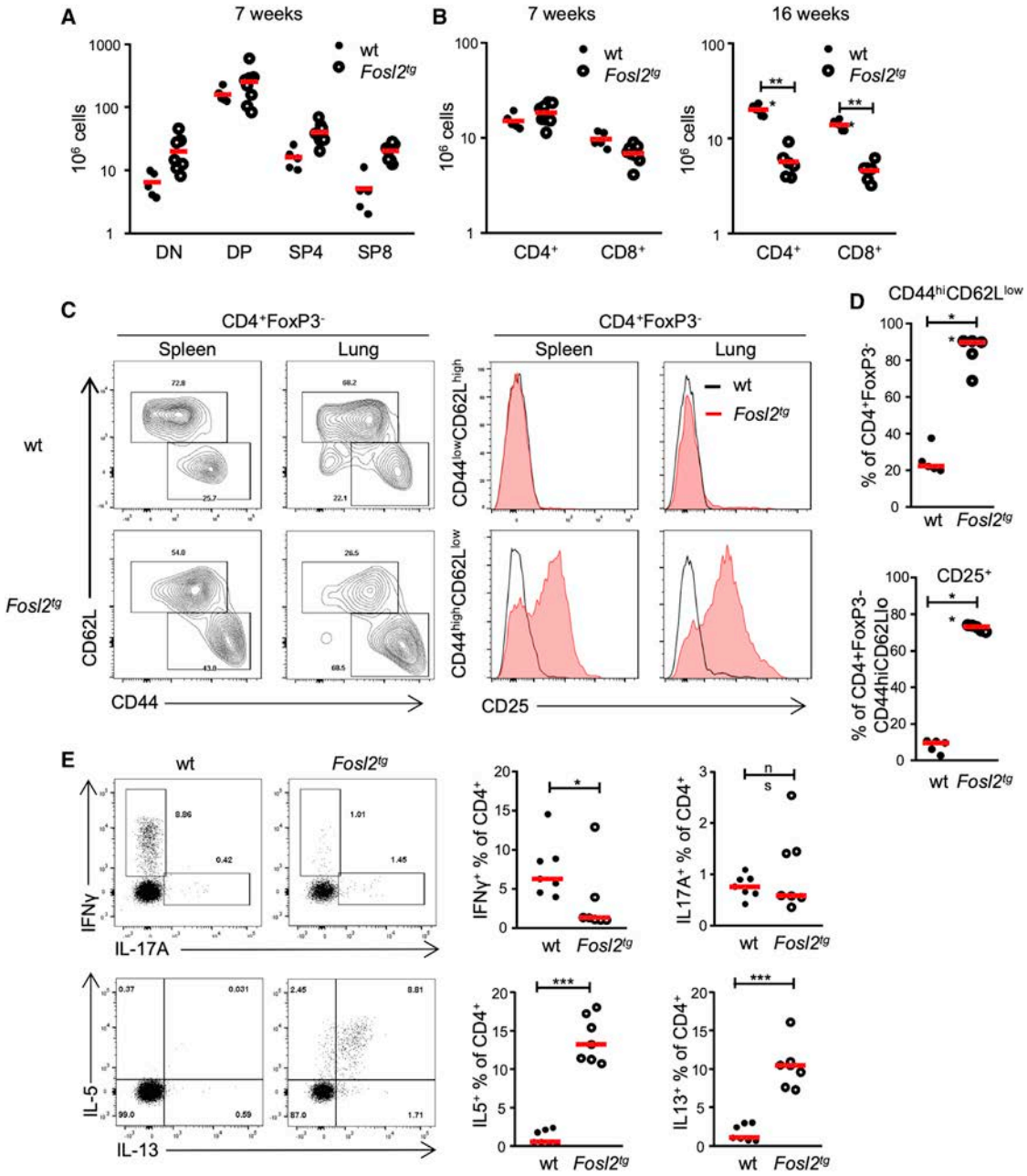

Figure 2. Increase of Effector T Cell Populations in Fosl2^{tg} Mice

(A) Quantification of cell populations in the thymus of 7-week-old WT and *Fosl2^{tg}* mice. DN, double-negative (CD4$^-$CD8$^-$); DP, double-positive (CD4$^+$CD8$^+$); CD4 SP, CD4$^+$ single-positive; CD8 SP, CD8$^+$ single-positive. n = 5–8.

(B) Quantification of T cells in the spleens of WT and *Fosl2^{tg}* mice at 7 or 16 weeks (n = 5–8).

(C) Analysis of the populations of activated (CD62L^{low}CD44^{hi}FoxP3$^-$) and naive (CD62L^{hi}CD44^{low}FoxP3$^-$) CD4$^+$ cells and expression of CD25 in these populations, from the lungs and spleens of WT or *Fosl2^{tg}* mice (females, 16 weeks old).

(D) Quantification of the cell populations as in (C) (n = 5 mice per group).

(E) Staining for cytokines in CD4$^+$ cells from WT and *Fosl2^{tg}* mice (females, 16 weeks old). Splenocytes were stimulated for 12 h with PMA/ionomycin in the presence of monensin and brefeldin A and stained for IFNγ, IL-17A, IL-5, and IL-13.

*p < 0.05, **p < 0.01, and ***p < 0.001, two-way ANOVA with Dunnett's multiple comparison (A and B) and Mann-Whitney test, two-tailed (D and E).

T cell development was largely normal, with only a slight increase in thymic cellularity (Figure 2A). There were also normal numbers of CD4$^+$ and CD8$^+$ T cells in the spleen (Figure 2B).

We then analyzed the phenotype of T cells in 16-week-old *Fosl2^{tg}* mice. We observed a significant drop in T cell numbers in the spleen at 16 weeks during the development of systemic

inflammation. In $CD4^+$ T lymphocytes, there was an accumulation of effector $CD62L^{low}CD44^{high}$ cells (Figures 2C and 2D), which also displayed increased CD25 expression, pointing to T cell activation. We also found a strong infiltration of T cells in the lungs and other affected organs. Naive T cells were also decreased, with an increase in activated T cells in the lungs (Figures 2C and 2D).

Given the clear T cell activation, we analyzed the profile of cytokines produced by these $CD4^+$ T cells in *Fosl2*^{tg} mice. There was a decrease in the population of IFNγ-secreting T cells and no significant change in the population of IL-17A-producing cells (Figure 2E; Figure S3D). However, we detected a strong increase in both the proportions and numbers of IL-5- and IL-13-positive cells, and the large majority were positive for both cytokines (Figure 2E; Figure S3D). These data confirm the presence of T cell activation in *Fosl2*^{tg} mice with systemic inflammation and show that these T cells are mostly Th2 polarized. This polarization is consistent with the inflammation we observed, in particular pulmonary eosinophilia and increased IgE and IL-5 in serum and skin lesions. Concomitantly, we found a decrease in Th1 cells with a strong drop in IFNγ-producing $CD4^+$ cells.

We also analyzed the $CD8^+$ T cell compartment, which showed a strong activation pattern, with a shift from a naive ($CD62L^{hi}CD44^{low}$) to an activated ($CD62L^{low}CD44^{hi}$) phenotype. In the spleen of *Fosl2*^{tg} mice, there was a decrease in the total number of IFNγ-positive cells (Figure S3E).

Fosl2 Represses Treg Development

A striking observation was that T cell activation in 16-week-old mice was paralleled by a strong decrease of the $CD25^+FoxP3^+$ Treg population in percentages and absolute numbers (Figure 3A). Interestingly, this decrease of Tregs in the spleen, inguinal lymph nodes (iLNs) and lungs in *Fosl2*^{tg} mice was already present at 3 weeks, before the appearance of T cell activation and before histological signs of organ inflammation (Figures 3B and 3C; Figures S5A–S5C). This confirmed that Treg decrease was constitutive in *Fosl2*^{tg} mice and not associated with a relative accumulation of non-Treg cells

Our next step was to check whether this Treg deficiency arises from an impairment of Treg development. Supporting this hypothesis, we could show that tTregs were also strongly decreased. Moreover, $CD4^+CD8^-CD25^+FoxP3^+$ tTregs were reduced but showed a normal pattern of CD44 and GITR expression (Figures 3D–3F and S5D). On the contrary, we observed that $CD4^+CD8^-CD25^+FoxP3^-$ tTreg precursors were present in normal amounts but showed an altered phenotype with a reduction of the $CD44^{hi}GITR^{hi}$ population, suggesting abnormal Treg development (Figures 3D–3F and S5D).

To further support a drop in tTreg production in Fosl2tg mice, we analyzed the expression of the tTreg marker Nrp1 in the periphery of young Fosl2tg mice. Interestingly we did find a decrease in the percentage of Nrp1-positive Tregs, consistent with our observation of decreased tTreg development (Figure S5E).

The abnormality in Treg development observed in the thymus of *Fosl2*^{tg} mice can explain the lack of Tregs in the periphery. However, it could also result from abnormal Treg homeostasis, with decreased proliferation or increased apoptosis. Thus, we analyzed Treg proliferation in *Fosl2*^{tg} mice. Surprisingly, *Fosl2*^{tg} Tregs were more proliferative than WT Tregs (Figure S7D). This increase in Treg proliferation might represent a compensatory mechanism in which the partially empty Treg niche promotes the proliferation of the remaining Tregs. We also analyzed Treg apoptosis in young Fosl2tg mice by staining the $CD4^+CD25^+$ population for annexin V. As expected, there were very few apoptotic Tregs, and there was no increase in *Fosl2*^{tg} mice (Figure S7E). Altogether, our data suggest that Treg homeostasis does not contribute to the Treg phenotype of *Fosl2*^{tg} mice.

We also assessed whether Fosl2 had an effect on the phenotype and suppressive function of Tregs. We thus analyzed *Fosl2*^{tg} Tregs for expression of several Treg-suppressive markers. Although there was a slight decrease in PD1 expression, CTLA4 was slightly increased, with no major changes in TIGIT, GITR, or CD62L expression (Figure S6A). Overall, Fosl2 had only a mild effect on Treg phenotype. We thus further addressed suppressive capacities of both Fosl2-deficient and Fosl2-overexpressing Tregs. Interestingly, they equally suppressed the proliferation of responder T cells (Figure S6B). These data suggest that Fosl2 is a repressor of Treg development but has little effect on their phenotype or suppressive function.

As the reduced number of Tregs might be responsible for the autoimmune phenotype of *Fosl2*^{tg} mice, we tested whether correction of the Treg deficiency would suppress the inflammatory phenotype. To this end, we used a T cell transfer setup in which total $CD4^+$ T cells from young *Fosl2*^{tg} mice were transferred to lymphopenic *Rag2*$^{-/-}$ hosts. We found that transfer of 1×10^6 purified $CD4^+$ T cells from young *Fosl2*^{tg} mice (5–7 weeks, before onset of T cell activation) into *Rag2*$^{-/-}$ recipients was sufficient to transfer the phenotype, as demonstrated by the development of severe lung inflammation within 5 weeks post-transfer (Figures 4A and 4B). This finding further supported the contribution of T cells to the inflammatory phenotype. We then tested the ability of co-transferred WT Tregs to suppress the inflammation induced by *Fosl2*^{tg} T cells. We first confirmed that Treg transfer restored a normal proportion of Tregs in recipient mice (Figure 4C). As expected, the supplementation of WT Tregs also resulted in a dose-dependent prevention of lung inflammation (Figures 4A and 4B). These data support the hypothesis that the decrease of the Treg population is causing the inflammation observed in *Fosl2*^{tg} mice.

Fosl2 Restricts Treg Development in a Cell-Intrinsic Manner

These experiments indicated that Fosl2 overexpression negatively affects the development of Tregs. We then tested whether this effect was bone marrow dependent. Irradiated *Rag2*$^{-/-}$ recipient mice were injected with sex-matched and T cell-depleted bone marrow from either WT or *Fosl2*^{tg} mice. Mice receiving *Fosl2*^{tg} bone marrow developed colitis about 35 days after transfer, as evidenced by weight loss, loose stools, reduction in colon length, and CD45 infiltrates in the colon (Figures 5A–5E). Moreover, we observed a decrease of Treg percentages in the thymus (Figure 5F). In the periphery, the lack of Tregs in recipients of *Fosl2*^{tg} bone marrow was even more pronounced than in *Fosl2*^{tg} mice (Figure 5G). Of note, *Fosl2*^{tg} mice did not develop colitis, a finding in contrast to our observation in mice

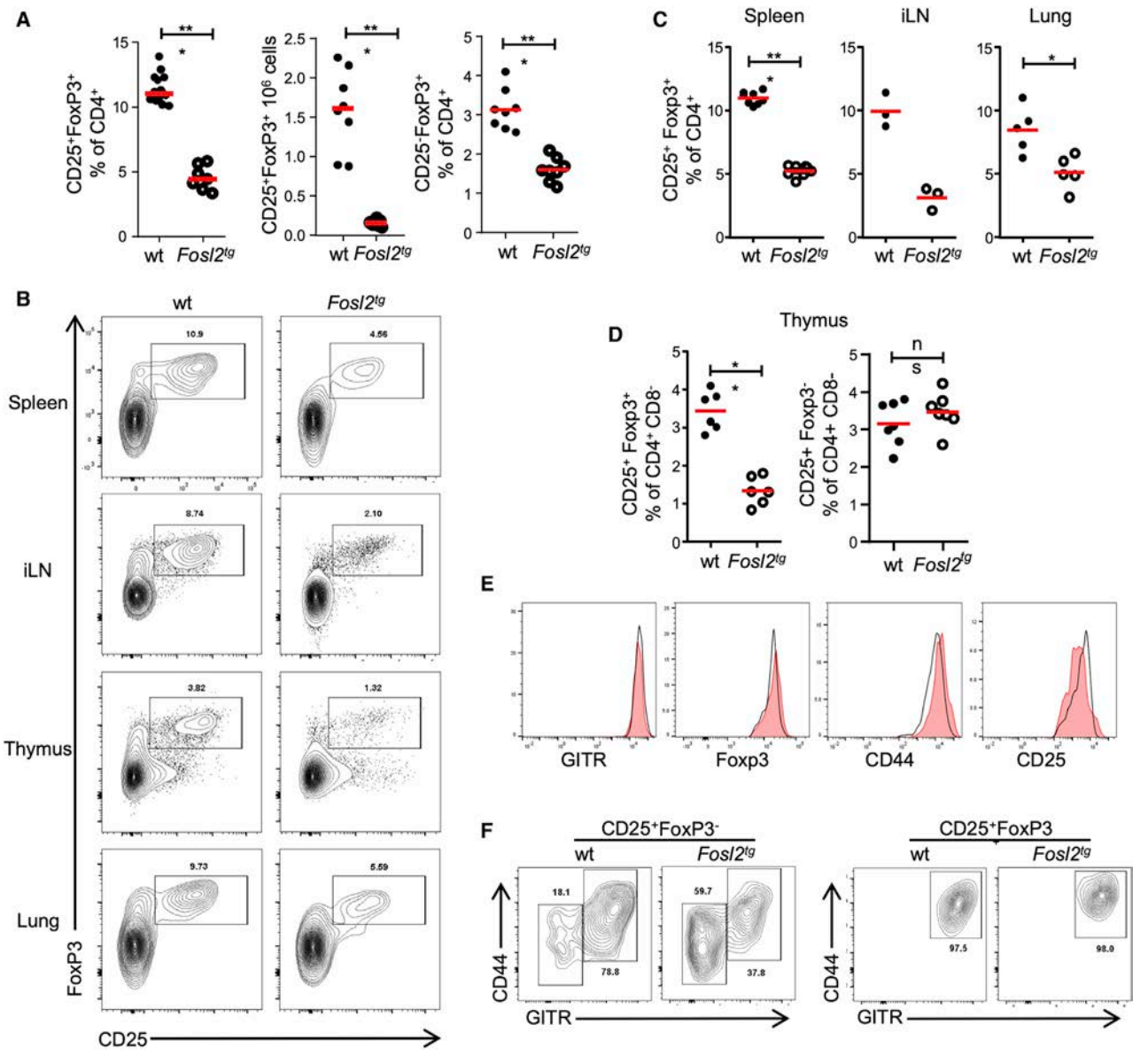

Figure 3. Treg Deficiency and Reduced tTreg Development in Fosl2^{tg} Mice

(A) Analysis of Treg populations (CD25$^+$FoxP3$^+$ and CD25$^-$FoxP3$^+$) within the CD4$^+$ T cells in the spleen of 16-week-old *Fosl2^{tg}* and WT mice (n > 7).

(B) Analysis of Treg population (CD25$^+$FoxP3$^+$) within CD4$^+$ T cells in the spleen, lung, inguinal lymph nodes (iLNs), and thymus in WT and *Fosl2^{tg}* mice (females, 3–6 weeks old).

(C) Quantifications of Tregs as in (B) (n = 3–8 mice per group).

(D) Analysis of CD25$^+$FoxP3$^-$ Treg precursors or CD25$^+$FoxP3$^+$ Tregs in CD4 SP cells of the thymus of WT or *Fosl2^{tg}* mice (3–6 weeks old).

(E) Analysis of GITR, FoxP3, CD44, and CD25 expression in tTregs from WT or *Fosl2^{tg}* mice (females, 3–6 weeks old).

(F) GITR and CD44 expression in either CD25$^+$FoxP3$^-$ Treg precursors or CD25$^+$FoxP3$^+$ Tregs in CD4 SP cells of the thymus of WT or *Fosl2^{tg}* mice (3–6 weeks old).

*p < 0.05, **p < 0.01, ***p < 0.001, Mann-Whitney test, two-tailed (A, C, and F).

receiving *Fosl2^{tg}* bone marrow. However, irradiated *Rag2$^{-/-}$* recipients represent a lymphopenic environment, which, combined with the Treg deficiency associated with *Fosl2^{tg}* bone marrow, explains the development of colitis.

To further support these findings, we transferred WT bone marrow into *Rag2$^{-/-}$ Fosl2^{tg}* mice, a setup in which WT thymocytes develop in a *Fosl2^{tg}* thymus. These chimeric mice did not develop colitis and had normal Treg populations in the thymus and in the periphery, confirming a bone marrow-dependent phenotype (Figures 5A–5G). Taken together, these data showed that the effect of Fosl2 on Treg development is bone marrow dependent.

Next, we addressed whether Fosl2 inhibits Treg development in a cell-intrinsic manner. To this end, we performed a mixed

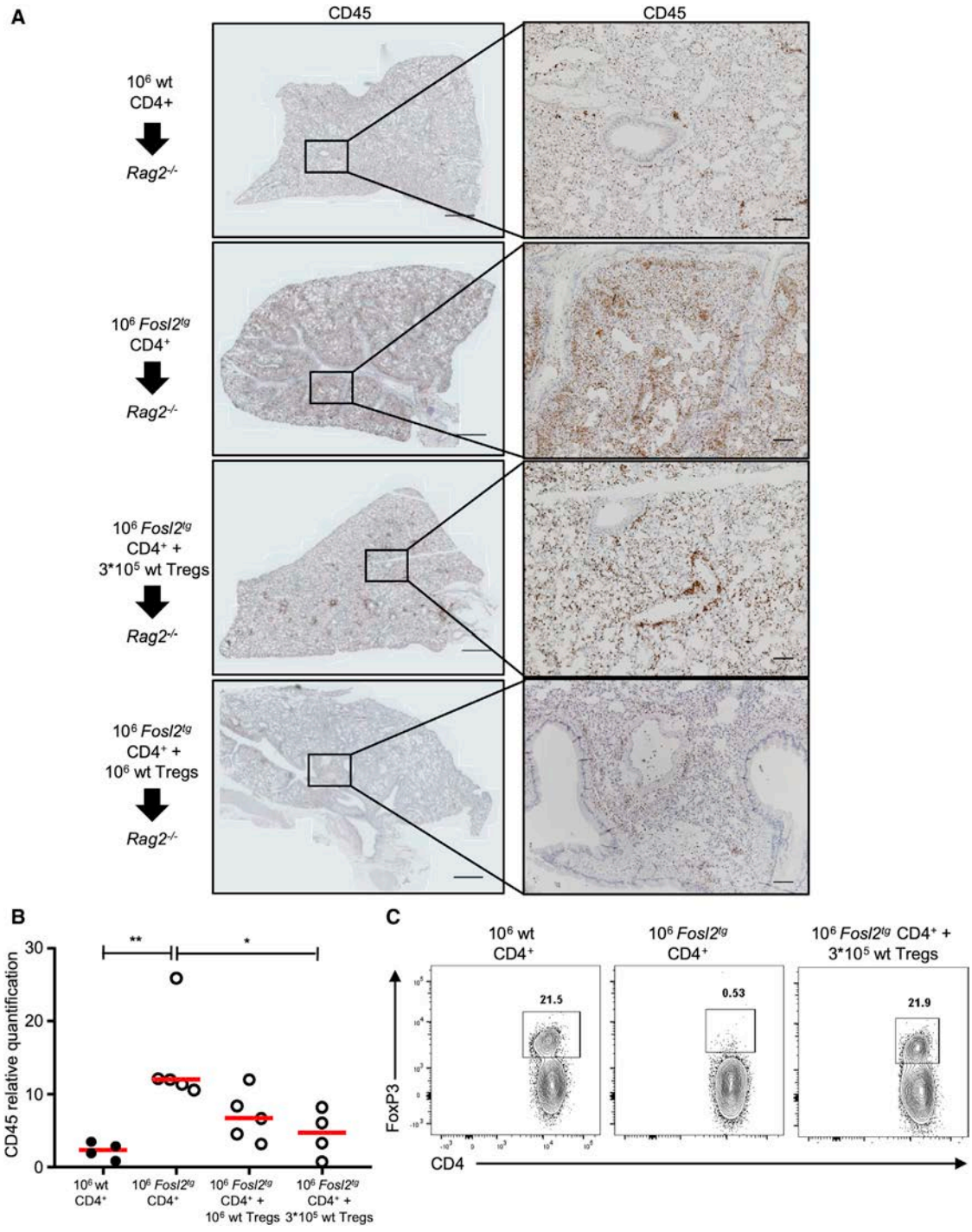

Figure 4. WT Tregs Suppress Lung Inflammation Induced by Fosl2^{tg} CD4$^+$ T Cells

(A) *Rag2*$^{-/-}$ mice (10–14 weeks old) received by intravenous (i.v.) injection 1 × 10^6 CD4$^+$ cells from WT mice or 1 × 10^6 CD4$^+$ cells from *Fosl2*^{tg} mice (4–6 weeks old) either alone or together with 3 × 10^5 or 10^6 Tregs from WT mice. Lungs were harvested 5 weeks after transfer, and paraffin-embedded lung sections were stained for CD45. Representative pictures of an entire lobe (left; scale bar, 1 mm) and higher magnification (right; scale bar, 100 μm).

(B) Relative quantification of CD45 staining of the lungs as in (A). Number of CD45-positive pixels was quantified in the entire lung sections and normalized to the total surface of the lung sections.

(C) FoxP3$^+$ cells in the spleens of recipients mice 5 weeks post-transfer show reconstitution of the Treg population by co-transfer of WT Tregs.

*p < 0.05 and **p < 0.01, Kruskal-Wallis test with Dunn's multiple testing.

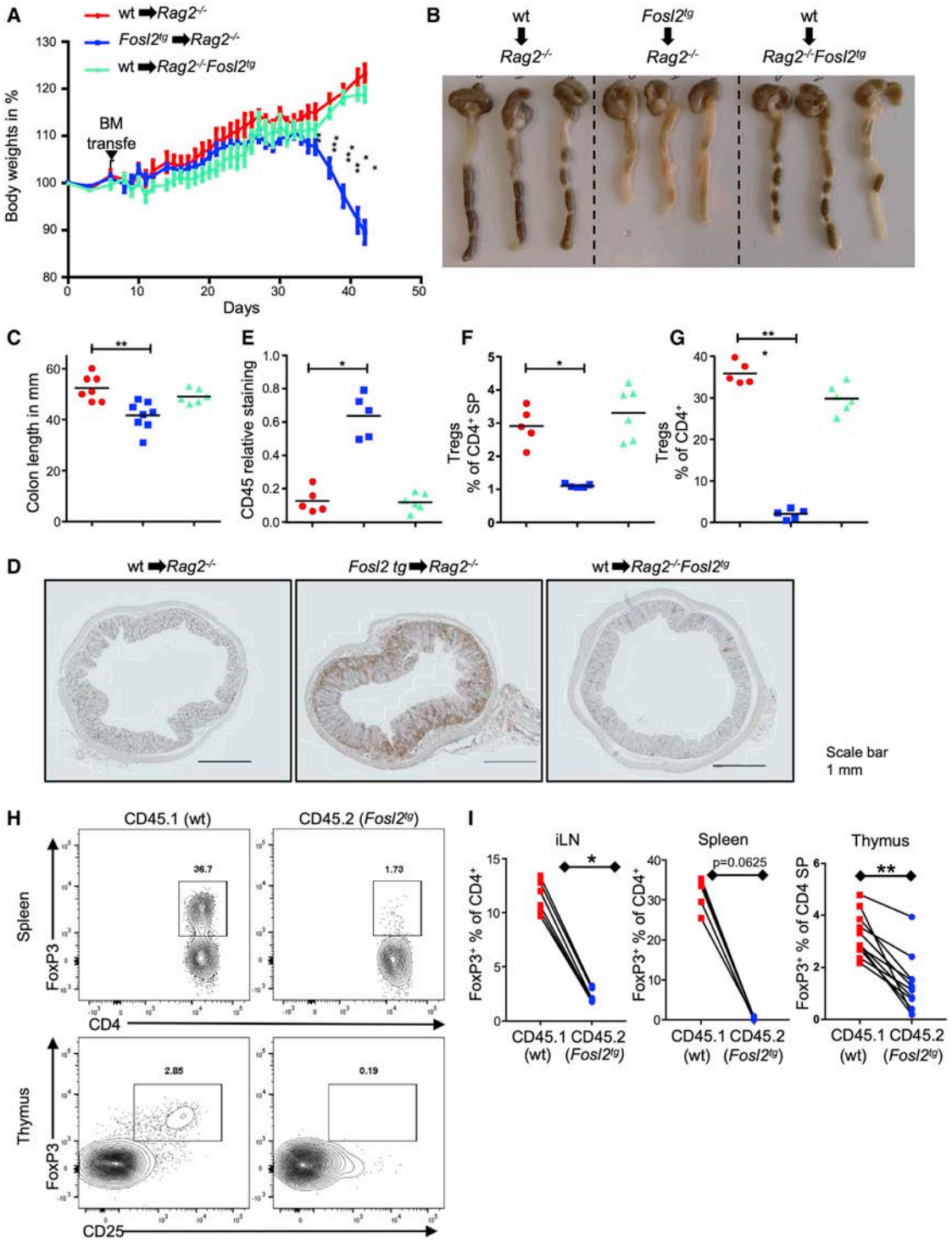

Figure 5. Fosl2 Effect on Tregs Is Bone Marrow Dependent

(A–G) Rag2$^{-/-}$ recipients (10–14 weeks old) received bone marrow from either WT or *Fosl2*^{tg} mice, and *Rag2*$^{-/-}$*Fosl2*^{tg} recipients received bone marrow from WT mice. Body weight changes in mice after transfer were recorded for 35 days (n = 5 or 6). (B) Representative pictures of colons at day 35 post-transfer. (C) Colon lengths as in (B). (D) Representative pictures of paraffin-embedded sections of the colon of mice as in (B) stained for CD45; scale bar, 1 mm. (E) Relative quantification of CD45 staining of the colon as in (D) (n $\geq$ 5). (F and G) Percentage of CD25^{+}FoxP3^{+} within the CD4^{+}CD8^{-} population in the thymus (F) and the spleen (G) of mice at day 35 post-transfer (n $\geq$ 5).

(legend continued on next page)

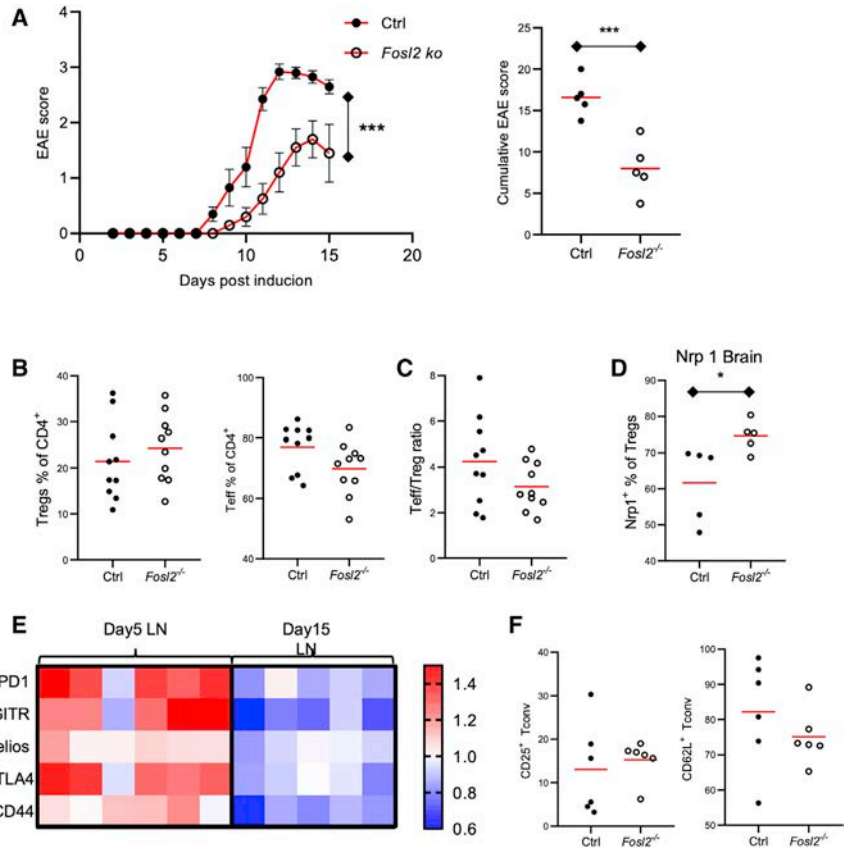

Figure 6. Deletion of Fosl2 in T Cells Reduces EAE Severity

(A) Fosl2$^{fl/fl}$CD4-Cre^{+} mice or Fosl2$^{fl/+}$CD4-Cre^{+} mice received a single immunization with MOG peptide to induce EAE. Mice were then scored for symptoms severity by a blinded observer. Data are representative of two different experiments with five mice per group in each.

(B) Treg and Teff populations of CD4^{+} cells were analyzed in the brain of EAE mice 15 days after immunization.

(C) Ratio of effectors to Treg cells in the brain as in (B).

(D) Percentage of Nrp1^{+} Tregs in the brain of EAE mice as in (B).

(E) Treg populations in the inguinal lymph nodes of EAE mice 5 or 15 days after immunization. Expression of Treg markers PD1, GITR, Helios, and CTLA4 and activation marker CD44 were analyzed. Fold change of expression in Fosl2$^{-/-}$ Tregs compared with control is represented.

(F) Expression of activation markers CD25 and CD62L by FoxP3^{-}CD4^{+} T cells in the lymph nodes of EAE mice 5 days after immunization.*p < 0.05, ***p < 0.001, Mann-Whitney test, two-tailed *p < 0.005.

bone marrow transfer, in which *Rag2*$^{-/-}$ recipients received a 1:1 mix of WT (CD45.1) and *Fosl2*^{tg} (CD45.2) sex-matched and T cell-depleted bone marrow. Interestingly, there was no overt colitis in these mice compared with recipients of pure *Fosl2*^{tg} bone marrow (Figure S7A), suggesting that WT bone marrow had a dominant protective effect. Strikingly, the proportion of FoxP3^{+} cells was much lower in *Fosl2*^{tg} CD4 SP cells compared with WT CD4 SP cells, confirming a cell-intrinsic effect of Fosl2. Here again, the proportion of FoxP3^{+} cells of *Fosl2*^{tg} origin in the periphery was much lower than in the *Fosl2*^{tg} mice (Figures 5H and 5I). We also directly compared the T cell development of WT versus *Fosl2*^{tg} cells in this mixed setup, and, confirming our data in *Fosl2*^{tg} mice, we did not detect a significant effect of Fosl2 on T cell development (Figures S7B and S7C). Altogether, we showed that Fosl2 overexpression inhibits, in a cell-intrinsic manner, tTreg development.

Fosl2 Deletion in T Cells Reduces Autoimmunity

Of note, mice with a T cell-specific Fosl2 deletion were reported to have a normal phenotype, without changes in T cells and Treg development or T cell populations in the periphery (Lawson et al., 2009). We could confirm these findings in our Fosl2$^{fl/fl}$ CD4-cre mice (Figures S8A and S8B).

To further address the effect of Fosl2 deletion in T cells, we first tested whether Fosl2ko T cells had different T cell development of homeostatic properties. To this end, we generated Fosl2ko-WT bone marrow chimera mice. In this setup, we observed a normal population of *Fosl2*$^{-/-}$ Tregs compared with WT (Figure S9A).

We next addressed whether a phenotype could be observed outside of steady-state conditions. We thus induced experimental autoimmune encephalomyelitis (EAE) in Fosl2$^{fl/fl}$CD4-cre mice to see if Fosl2 deletion altered autoimmunity. Strikingly, Fosl2 deletion significantly reduced the severity of EAE, which mirrored our observations of spontaneous autoimmunity in *Fosl2*^{tg} mice (Figure 6A).

We further analyzed the composition of the T cell population in mice with EAE. There was no significant change in the Treg population in the brains of Fosl2-deficient EAE mice. There was a tendency toward a lower proportion of effector cells, and a lower Teff-to-Treg ratio, which might be due to the overall decreased severity of inflammation in Fosl2ko mice (Figures 6B and 6C). Interestingly, there was an increase in the expression of the tTreg marker Nrp1 in the brains of Fosl2-deficient mice (Figure 6D). This

(H) *Rag2*$^{-/-}$ recipients (10–14 weeks old) received mixed 1:1 bone marrow (WT, CD45.1; *Fosl2*^{tg}, CD45.2). Representative plot of FoxP3 staining in the spleen within CD4^{+} cells and within the CD4^{+}CD8^{-} populations in the thymus of either CD45.1 (WT) or CD45.2 (*Fosl2*^{tg}) origin in recipient mice at day 35 post-transfer.

(I) Percentages of FoxP3^{+} cells within CD4^{+} (iLN and spleen) or within CD4^{+}CD8^{-} (thymus) cells as in (H).

*p < 0.05, **p < 0.01, and ***p < 0.001, two-way ANOVA with Tukey's multiple comparison test (A), Kruskal-Wallis test with Dunn's post hoc analysis (B–D), and Wilcoxon test, two-tailed (I).

finding is supportive of our observation of reduced tTregs in *Fosl2*^{tg} mice. We then hypothesized that Fosl2 deficiency might affect the induction phase in EAE, and we analyzed the population of Tregs in the iLNs 5 days after immunization. There, we observed an overall tendency toward an increase in all Treg-suppressive markers that we analyzed (Figures 6E, S9B, and S9C). On the other hand, these markers were decreased later during the disease, at a stage when Fosl2ko mice had reduced disease severity.

To address the possibility that reduced EAE severity is due to a reduction in T cell activation, we first tested *in vitro* the effect of Fosl2 on T cell activation. We did not obverse any significant changes in the expression of activation markers or proliferation of anti-CD3/anti-CD28 stimulated T cells upon overexpression or deletion of Fosl2 (Figures S8C and S8D). We also did not observe a change in conventional T (Tconv) cell activation markers in EAE mice (Figure 6F).

We thus demonstrate that Fosl2 deficiency in T cells results in a clear reduction in autoimmunity, with a slight modification of the Treg population and an increase in Nrp1^{+} Tregs.

Fosl2 Is TCR Induced and Reduces FoxP3 Expression

To address how Fosl2 affects Treg development, we first analyzed Fosl2 expression in T cells. Whereas Fosl2 protein could not be detected in unstimulated naive T cells, Fosl2 mRNA was rapidly upregulated 30 min after TCR stimulation and reached a plateau thereafter (Figure S10A). This resulted in a strong upregulation at the protein level after 24 h (Figure 7A). Expression of Fosl2 was delayed in comparison with Fos and Jun. To address whether Fosl2 was also induced by TCR signaling in developing thymocytes, Fosl2 expression was quantified in CD69^{-} and CD69^{+} double-positive (DP) thymocytes, corresponding to earliest TCR signaling in thymocytes. There was a strong upregulation of Fosl2 mRNA in CD69^{+} DP thymocytes, confirming that Fosl2 expression is induced by TCR (Figure 7B), a finding supported by available proteomic datasets (Tan et al., 2017).

As Fosl2 was reported to be differentially expressed in Th1 and Th2 cells, and is a Stat3 target gene during Th17 induction (Tripathi et al., 2017; Lund et al., 2007), we analyzed how polarizing conditions would further affect Fosl2 protein expression. We stimulated CD4^{+} T cells for 24 h with anti-CD3 and anti-CD28 monoclonal antibodies (mAbs) under Th0, Th1, Th2, Th17, and iTreg conditions. There was little difference in Fosl2 expression during Th cell polarization, with a slightly lower expression in Th2 (Figure 7C), but Fosl2 expression was decreased under iTreg conditions. The reduced expression of Fosl2 was confirmed in Tregs and their precursors isolated from the thymus (Figure 7D).

To support our findings and address whether Fosl2 expression pattern is similar in humans, we used an available dataset of RNA sequencing (RNA-seq) in multiple immune cell populations sorted from human healthy blood (Schmiedel et al., 2018). Interestingly, there was a clear upregulation of Fosl2 after TCR stimulation, similar to what we observed in mice (Figure 7E). Moreover, Fosl2 expression was lower in Tregs, especially naive Tregs, with Th1 and Th17 showing higher expression (Figure 7E). We also found that compared with other AP1 members, the expression pattern of Fosl2 was unique. Indeed, Fosl2 shows the most differential expression in the different T cell subsets among all AP1 proteins and is, with Fosl1, the only one still upregulated on mRNA level after 4 h (Figure S10B).

We next investigated the mechanisms by which Fosl2 represses Treg development. As Fosl2 target genes in T cells were so far unknown, we addressed the effect of Fosl2 on the transcriptome of T cells during T cell activation.

Sorted naive (CD62L^{high}CD44^{low}CD25^{-}) CD4^{+} T cells from WT, *Fosl2*^{tg}, or *Fosl2*$^{fl/fl}$CD4-cre^{+} mice (hereafter *Fosl2*$^{-/-}$) were stimulated *in vitro* for 24 h with anti-CD3 and anti-CD28 mAbs. The mRNA expression profile was analyzed using RNA-seq.

We first confirmed the efficacy of Fosl2 overexpression and depletion by analyzing reads over the Fosl2 loci (Figure S10C).

We ran pairwise comparisons to establish a list of differentially expressed genes (corrected $p < 0.05$) among WT, *Fosl2*^{tg}, and *Fosl2*$^{-/-}$. We then filtered genes with fold changes > 1.5 and applied a false discovery rate of 5%. We further focused on genes with opposite regulation in *Fosl2*^{tg} versus *Fosl2*$^{-/-}$. This strategy yielded 189 Fosl2-regulated genes (Figure 7F).

FoxP3 was one of the top differentially regulated genes, with a clear downregulation in *Fosl2*^{tg} cells and upregulation in *Fosl2*$^{-/-}$ cells (Figure 7G). This result supported our hypothesis and confirmed that the level of Fosl2 expression during T cell activation controls the expression of FoxP3. We then assessed whether Fosl2 also affected expression of FoxP3 on the protein level. We analyzed the percentage of FoxP3-positive cells after 3 days of activation without or with 1 ng/mL TGF-β. In the absence of TGF-β, there were very few FoxP3-positive cells, with, however, a small increase in FoxP3-positive cells in *Fosl2*$^{-/-}$ cells (Figure 7G). In contrast, in the presence of TGF-β, *Fosl2*^{tg} cells had a clear reduction in FoxP3, confirming that Fosl2 also repressed iTreg induction. To further address whether Fosl2 could affect FoxP3 expression, we compared FoxP3 mean fluorescence intensity (MFI) in mixed bone marrow chimera mice that received a mix of either WT and *Fosl2*^{tg} or WT and *Fosl2*$^{fl/fl}$*Cd4-cre*$^{+}$ bone marrow. In this setup, WT cells serve as an internal control to precisely compare the level of FoxP3 expression (Figure 7I). We confirmed that Fosl2 overexpression reduced FoxP3 expression in Tregs. In *Fosl2*$^{-/-}$ Tregs, there was also a slight increase in FoxP3 MFI compared with WT, although the magnitude of this change was very small (Figure 7I).

Fosl2 also repressed the expression of Nr4a2, IRF8, Ccl1, and Ccr8 (Figure S10D), four genes involved in Treg differentiation or function (Sekiya et al., 2011; Lee et al., 2016; Barsheshet et al., 2017).

To further analyze the effects of Fosl2 on the T cell transcriptome, we ranked Fosl2-regulated genes using the sum of fold changes in *Fosl2*^{tg} and *Fosl2*$^{-/-}$ T cells compared with WT. We then ran a pre-ranked gene set enrichment analysis (GSEA) to compare our gene set with previously published immunologic gene sets of the GSEA database (Subramanian et al., 2005; Mootha et al., 2003). Interestingly, among the first ten datasets enriched in our gene list, three were linked to FoxP3-transduced cells and two with tTreg development. In particular, four datasets reached a false discovery rate of 0.05 (Figure S10F). Strikingly, the most significant dataset showed a negative correlation between Fosl2-promoted genes and the tTreg gene signature

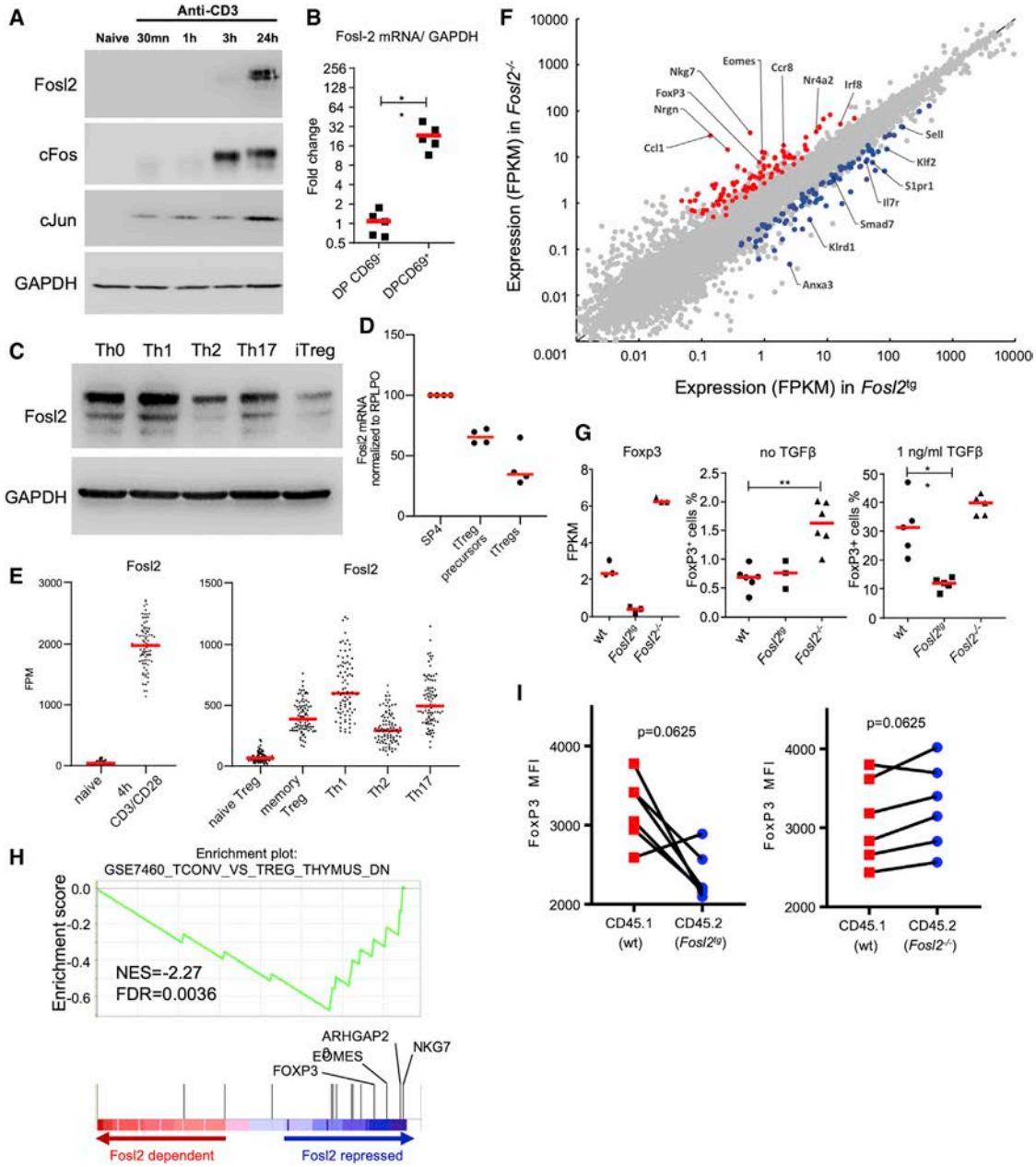

Figure 7. Fosl2 Controls FoxP3 Expression and Treg Signature

(A) Sorted naive CD4$^+$CD25$^-$CD62L^{low}CD44^{hi} T cells were stimulated and Fosl2 expression was analyzed by immunoblot. Representative of n = 3 biological replicates.

(B) qPCR analysis of Fosl2 expression in thymocyte populations (DP, double-positive CD4$^+$CD8$^+$), normalized to GAPDH; n = 5 biological replicates.

(C) WT CD4$^+$ T cells were stimulated for 24 h with anti-CD3 (2 μg/mL) and anti-CD28 (2 μg/mL) mAbs in Th0-, Th1-, Th2-, Th17-, or iTreg-polarizing conditions. Western blot with GAPDH as loading control. Representative of n = 3 biological replicates.

(D) Fosl2 mRNA expression in FoxP3$^+$CD25$^+$ (tTreg) and FoxP3$^-$CD25$^+$ tTreg precursors compared with single-positive (SP4) thymocytes in FoxP3-GFP mice.

(E) Fosl2 expression in human healthy T cells sorted from blood (publicly available dataset; Schmiedel et al., 2018).

(F) Gene expression as FPKM in *Fosl2^{tg}* versus *Fosl2$^{-/-}$* T cells. Sorted naive (CD62L^{high}CD44^{low}CD25$^-$) CD4$^+$ T cells from WT, *Fosl2^{tg}*, or *Fosl2$^{fl/fl}$*CD4-cre$^+$ mice (referred to as *Fosl2$^{-/-}$*) were stimulated for 24 h with anti-CD3 and anti-CD28. Genes repressed by Fosl2 (i.e., downregulated in *Fosl2^{tg}* cells and upregulated in *Fosl2$^{-/-}$* cells) are highlighted in red. Genes promoted by Fosl2 are highlighted in blue.

(G) FPKM expression of FoxP3 in our RNA-seq experiment and FoxP3 expression by fluorescence-activated cell sorting (FACS) in *Fosl2^{tg}* and *Fosl2$^{-/-}$* T cells after 3 days of stimulation with or without TGF-β.

(H) Enrichment plot for the dataset GSE7460.

(I) Comparison of FoxP3 expression (MFI) by FACS in Tregs of WT, *Fosl2^{tg}*, or *Fosl2$^{fl/fl}$*CD4-cre$^+$ origin in mixed bone marrow transferred mice.

(Figure 7H). Altogether, these data confirm that the level of Fosl2 expression can repress the expression of FoxP3 and of Treg-specific genes during the development of Tregs.

DISCUSSION

Tregs are crucial in maintaining homeostasis and tolerance in the immune system. Alterations in pathways controlling the development and function of Tregs have been proposed to be important pathomechanisms in autoimmune and auto-inflammatory diseases. Here we have discovered that the AP1 transcription factor Fosl2 is central to the control of autoimmunity and is involved in Treg development.

Fosl2^{tg} mice showed similarities with the phenotype of fully Treg-deficient Scurfy and DEREG mice and the disease developed by IPEX patients. However, *Fosl2*^{tg} animals survived longer and had a less severe phenotype, which might be explained by the partial Treg deficiency in *Fosl2*^{tg} animals (Brunkow et al., 2001; Godfrey et al., 1991; Lahl et al., 2007). The inflammation observed in the lungs, skin, liver, pancreas, and salivary glands is also strikingly similar to what was observed in mice with Treg-specific genetic disruptions (Miyazaki et al., 2014) and is reminiscent of the organ inflammation observed in several autoimmune diseases.

Our data in *Fosl2*^{tg} mice suggest that the reduction of the Treg population is caused mostly by a decrease in tTreg development. We indeed observed a reduction in the tTreg population, while the composition of the tTreg precursor population was altered. However, the increased proliferation rate of *Fosl2*^{tg} Tregs observed in T cell transfer or bone marrow transfer experiments suggests that under certain circumstances, Fosl2 might also control Treg homeostasis.

Our data also support the idea that Fosl2 can affect the expression of FoxP3 on both mRNA and protein levels. However, we cannot definitely establish whether Fosl2's control of FoxP3 is direct or indirect. For example, we identified in our RNA-seq experiment a set of genes modulated by Fosl2 and known to contribute to Treg biology. In particular, Fosl2 repressed the expression of Nr4a2 and IRF8, two transcription factors involved in Treg differentiation or function (Sekiya et al., 2011; Lee et al., 2016). Furthermore, Fosl2 repressed Ccl1 and its receptor Ccr8. Interestingly, Ccr8^{+} Tregs have been shown to be important in immune regulation through autocrine stimulation of Tregs by Ccl1 (Barsheshet et al., 2017).

On the other hand, AP1 is known to function as a network of heterodimers, and the Fos/Jun dimers in particular are known to promote the expression of FoxP3 through direct binding to FoxP3 promotor (Ogawa et al., 2014). One possible mechanism would thus be that Fosl2, when forming dimers with other AP1 members, can directly interact with FoxP3 locus and repress transcription. This could counter, or compete with, the effects of other AP1 dimers such as Jun/Fos, which normally promote FoxP3 expression.

Such a mechanism of action can also be discussed in light of our observations in T cell-specific Fosl2-deficient mice. Indeed, we did not observe a phenotype under steady-state conditions, which would indicate that Fosl2 is not involved in T cell biology. This apparent lack of phenotype is not completely surprising given the complex and partly redundant mode of action within the AP1 family. There have indeed been several examples of functional redundancies in the AP1 family and in particular among the Fos proteins. Fos is a good example of this, as its role in T cell biology is well described, with the Fos/Jun AP1 complex, for example, being key in the induction of IL-2 or FoxP3 expression (Ogawa et al., 2014; Ochi et al., 1994; Jain et al., 1992). However, as for Fosl2 in our study, T cell-specific Fos-knockout mice have no apparent phenotype with normal T cell development and normal T cell function in the periphery (Jain et al., 1994). Fos-knockout T cells also express normal amounts of IL-2 despite the important role of c-Fos in IL-2 expression. On the contrary, c-Fos overexpression leads to a strong (>5-fold) increase in IL-2 expression (Ochi et al., 1994), indicating that overexpression is an important tool to highlight AP1 protein functions. Further supporting this, replacing c-Fos gene by Fosl1 in mice has no phenotypic consequences, confirming that c-Fos and Fosl1 have maintained a functional equivalence (Fleischmann et al., 2000). We thus think that as for Fos, other AP1 members can partially compensate the loss of Fosl2 and explain our observations in Fosl2$^{fl/fl}$CD4-cre mice under steady state.

Importantly, our findings in the EAE model, in which we observed a clear reduction in autoimmunity upon T cell-specific deletion of Fosl2, confirm that Fosl2 is important in T cell-mediated control of tolerance. Under these autoimmune conditions, which represent a dynamic situation with T cell activation, it seems that the function of Fosl2 is not fully compensated, enabling us to observe Fosl2 contribution to AP1-mediated control of T cell tolerance. Our findings thus suggest that in T cells, Fosl2 has both a set of unique functions, visible in our EAE experiments, and redundant functions, which mitigate the phenotype of Fosl2 depletion. It would be interesting to further dissect the contribution of other AP1 members to understand which one mediates this redundancy. Of note, there is so far no report of the function of Fosl1, which has an 85% homology to Fosl2, in T cells. Fosl1 might thus be a good candidate to investigate the redundancy with Fosl2 functions.

Interestingly, we also found that *Fosl2*^{tg} mice develop a strongly Th2-polarized autoimmune response. This polarization might indicate an additional function for Fosl2 in effector T cell polarization. This is in line with other observations indicating the contribution of AP1 members to Th cell biology (Carr et al., 2017). Moreover, this Th2 polarization might partly explain the organs affected by autoimmunity in *Fosl2*^{tg} mice. The lungs and skin, which are heavily inflamed in *Fosl2*^{tg} mice, are indeed prone to Th2 inflammation, while the colon, for example, which is often affected by Th1- and Th17-dependent inflammation in the absence of Tregs, is not affected in our mice (Feng et al., 2011).

We have found that Fosl2 is a TCR-induced gene in both thymocytes and mature T cells, with lower expression in Tregs. Interestingly this was common to both human and mice. This suggests that Fosl2's ability to influence inflammation and autoimmunity could also be relevant in humans. Supporting that fact, several GWASs reported association of a SNP within the promoter of Fosl2 with risk for inflammatory bowel disease (IBD) and allergic diseases (Jostins et al., 2012; Liu et al., 2015; Ye and McGovern, 2016; Ferreira et al., 2019). Moreover, this SNP

was shown to correlate with Fosl2 expression in blood cells of IBD patients (Di Narzo et al., 2016), indicating that Fosl2 risk association is mediated by immune cells. Also supporting the clinical relevance of Fosl2 expression in Tregs, it was found that Fosl2 is a determinant of a highly suppressive subpopulation of Tregs in humans, which are enriched in the lamina propria of Crohn's disease patients and which support wound repairs in the mucosa (Povoleri et al., 2018).

In summary, we present significant evidence that Fosl2 is an important AP1 member involved in the repression of Treg development, with direct effects on autoimmunity and inflammation. *Fosl2*^{tg} mice will also constitute a valuable model to study how Treg deficiency triggers autoimmunity and inflammatory organ involvement or to address sex differences in susceptibility to immune tolerance breakdown.

DATA AVAILABILITY

RNA-seq data accession code Gene Expression Omnibus: GSE132313.

STAR★METHODS

Detailed methods are provided in the online version of this paper and include the following:

- KEY RESOURCES TABLE
- RESOURCE AVAILABILITY
  - Lead Contact
  - Materials Availability
  - Data and Code Availability
- EXPERIMENTAL MODEL AND SUBJECT DETAILS
  - Animals
- METHOD DETAILS
  - Experimental Autoimmune Encephalomyelitis
  - Flow cytometry
  - Histology and Immunohistochemistry
  - Cell culture
  - RT-qPCR
  - Western-blot
  - ELISA and multiplex
  - RNA-sequencing
  - Imaging and immunohistochemistry quantification
  - T cell transfer
  - Bone marrow transfer
  - Treg suppression assay
  - T cell polarizing conditions
- QUANTIFICATION AND STATISTICAL ANALYSIS

SUPPLEMENTAL INFORMATION

Supplemental Information can be found online at https://doi.org/10.1016/j.celrep.2020.107826.

ACKNOWLEDGMENTS

We thank Professor Aline Bozec for providing the Fosl2 floxed mice. This work was supported by the Rare Disease Initiative Zurich, SwissLife, the University of Zurich Forschungskredit, EMDO, and the Kurt und Senta Herrmann Stiftung.

AUTHOR CONTRIBUTIONS

O.D. directed the project. O.D., M.O.B., and F.R. obtained funding. O.D. and F.R. designed, analyzed, and interpreted experiments and wrote the manuscript. F.R. performed experiments with help from M.S. for mouse work and organ isolation and help from C.H. for experiments on *Fosl2*$^{fl/fl}$CD4-cre mice. A.V. provided histopathological analysis. R.H. and A.S. provided *Fosl2*^{tg} mice and performed multiplex experiments. G.K. helped in mouse experiment planning, design, and ethical applications. P.B., B.B., J.H.W.D., M.O.B., and O.B. participated in the design, analysis, and interpretation of the experiments.

DECLARATION OF INTERESTS

O.D. had consultancy relationships and/or has received research funding from A. Menarini, Acceleron Pharma, Amgen, AnaMar, Bayer, Boehringer Ingelheim, Catenion, CSL Behring, ChemomAb, Ergonex, GSK, Inventiva, Italfarmaco, iQone, iQvia, Lilly, medac, Medscape, Mitsubishi Tanabe Pharma, Merck Sharpe & Dohme (MSD), Novartis, Pfizer, Roche, Sanofi, Blade Therapeutics, CSL Behrings Target Bio Science, and UCB in the area of potential treatments for scleroderma and its complications. In addition, Prof. Distler has a patent mir-29 for the treatment of systemic sclerosis (US8247389, EP2331143). R.H. and A.S. are full-time employees of Sanofi-Genzyme.

Received: October 14, 2019
Revised: March 27, 2020
Accepted: June 5, 2020
Published: June 30, 2020

REFERENCES

Bao, R., Hou, J., Li, Y., Bian, J., Deng, X., Zhu, X., and Yang, T. (2016). Adenosine promotes FoxP3 expression in Treg cells in sepsis model by activating JNK/AP-1 pathway. Am. J. Transl. Res. *8*, 2284–2292.

Barsheshet, Y., Wildbaum, G., Levy, E., Vitenshtein, A., Akinseye, C., Griggs, J., Lira, S.A., and Karin, N. (2017). CCR8^{+}FOXp3^{+} T_{reg} cells as master drivers of immune regulation. Proc. Natl. Acad. Sci. U S A *114*, 6086–6091.

Bennett, C.L., Christie, J., Ramsdell, F., Brunkow, M.E., Ferguson, P.J., Whitesell, L., Kelly, T.E., Saulsbury, F.T., Chance, P.F., and Ochs, H.D. (2001). The immune dysregulation, polyendocrinopathy, enteropathy, X-linked syndrome (IPEX) is caused by mutations of FOXP3. Nat. Genet. *27*, 20–21.

Bozec, A., Bakiri, L., Jimenez, M., Rosen, E.D., Catalá-Lehnen, P., Schinke, T., Schett, G., Amling, M., and Wagner, E.F. (2013). Osteoblast-specific expression of Fra-2/AP-1 controls adiponectin and osteocalcin expression and affects metabolism. J. Cell Sci. *126*, 5432–5440.

Bozec, A., Bakiri, L., Jimenez, M., Schinke, T., Amling, M., and Wagner, E.F. (2010). Fra-2/AP-1 controls bone formation by regulating osteoblast differentiation and collagen production. J. Cell Biol. *190*, 1093–1106.

Brunkow, M.E., Jeffery, E.W., Hjerrild, K.A., Paeper, B., Clark, L.B., Yasayko, S.A., Wilkinson, J.E., Galas, D., Ziegler, S.F., and Ramsdell, F. (2001). Disruption of a new forkhead/winged-helix protein, scurfin, results in the fatal lymphoproliferative disorder of the scurfy mouse. Nat. Genet. *27*, 68–73.

Carr, T.M., Wheaton, J.D., Houtz, G.M., and Ciofani, M. (2017). JunB promotes Th17 cell identity and restrains alternative CD4^{+} T-cell programs during inflammation. Nat. Commun. *8*, 301.

Chatila, T.A., Blaeser, F., Ho, N., Lederman, H.M., Voulgaropoulos, C., Helms, C., and Bowcock, A.M. (2000). JM2, encoding a fork head-related protein, is mutated in X-linked autoimmunity-allergic disregulation syndrome. J. Clin. Invest. *106*, R75–R81.

Chen, W., Jin, W., Hardegen, N., Lei, K.J., Li, L., Marinos, N., McGrady, G., and Wahl, S.M. (2003). Conversion of peripheral CD4+CD25− naive T cells to CD4+CD25+ regulatory T cells by TGF-beta induction of transcription factor FoxP3. J. Exp. Med. *198*, 1875–1886.

Ciofani, M., Madar, A., Galan, C., Sellars, M., Mace, K., Pauli, F., Agarwal, A., Huang, W., Parkhurst, C.N., Muratet, M., et al. (2012). A validated regulatory network for Th17 cell specification. Cell *151*, 289–303.

Di Narzo, A.F., Peters, L.A., Argmann, C., Stojmirovic, A., Perrigoue, J., Li, K., Telesco, S., Kidd, B., Walker, J., Dudley, J., et al. (2016). Blood and intestine eQTLs from an anti-TNF-resistant Crohn's disease cohort inform IBD genetic association loci. Clin. Transl. Gastroenterol. *7*, e177.

Eferl, R., Hasselblatt, P., Rath, M., Popper, H., Zenz, R., Komnenovic, V., Idarraga, M.H., Kenner, L., and Wagner, E.F. (2008). Development of pulmonary fibrosis through a pathway involving the transcription factor Fra-2/AP-1. Proc. Natl. Acad. Sci. U S A *105*, 10525–10530.

Eferl, R., Zenz, R., Theussl, H.C., and Wagner, E.F. (2007). Simultaneous generation of fra-2 conditional and fra-2 knock-out mice. Genesis *45*, 447–451.

Facciabene, A., Motz, G.T., and Coukos, G. (2012). T-regulatory cells: key players in tumor immune escape and angiogenesis. Cancer Res. *72*, 2162–2171.

Feng, T., Qin, H., Wang, L., Benveniste, E.N., Elson, C.O., and Cong, Y. (2011). Th17 cells induce colitis and promote Th1 cell responses through IL-17 induction of innate IL-12 and IL-23 production. J. Immunol. *186*, 6313–6318.

Ferreira, M.A.R., Vonk, J.M., Baurecht, H., Marenholz, I., Tian, C., Hoffman, J.D., Helmer, Q., Tillander, A., Ullemar, V., Lu, Y., et al. (2019). Eleven loci with new reproducible genetic associations with allergic disease risk. J. Allergy Clin. Immunol. *143*, 691–699.

Fleischmann, A., Hafezi, F., Elliott, C., Remé, C.E., Rüther, U., and Wagner, E.F. (2000). Fra-1 replaces c-Fos-dependent functions in mice. Genes Dev. *14*, 2695–2700.

Godfrey, V.L., Wilkinson, J.E., and Russell, L.B. (1991). X-linked lymphoreticular disease in the scurfy (sf) mutant mouse. Am. J. Pathol. *138*, 1379–1387.

Grant, C.R., Liberal, R., Mieli-Vergani, G., Vergani, D., and Longhi, M.S. (2015). Regulatory T-cells in autoimmune diseases: challenges, controversies and—yet—unanswered questions. Autoimmun. Rev. *14*, 105–116.

Hess, J., Angel, P., and Schorpp-Kistner, M. (2004). AP-1 subunits: quarrel and harmony among siblings. J. Cell Sci. *117*, 5965–5973.

Jain, J., Nalefski, E.A., McCaffrey, P.G., Johnson, R.S., Spiegelman, B.M., Papaioannou, V., and Rao, A. (1994). Normal peripheral T-cell function in c-Fos-deficient mice. Mol. Cell. Biol. *14*, 1566–1574.

Jain, J., Valge-Archer, V.E., and Rao, A. (1992). Analysis of the AP-1 sites in the IL-2 promoter. J. Immunol. *148*, 1240–1250.

Jostins, L., Ripke, S., Weersma, R.K., Duerr, R.H., McGovern, D.P., Hui, K.Y., Lee, J.C., Schumm, L.P., Sharma, Y., Anderson, C.A., et al. (2012). Host-microbe interactions have shaped the genetic architecture of inflammatory bowel disease. Nature *491*, 119–124.

Koizumi, S.I., Sasaki, D., Hsieh, T.H., Taira, N., Arakaki, N., Yamasaki, S., Wang, K., Sarkar, S., Shirahata, H., Miyagi, M., and Ishikawa, H. (2018). JunB regulates homeostasis and suppressive functions of effector regulatory T cells. Nat. Commun. *9*, 5344.

Lahl, K., Loddenkemper, C., Drouin, C., Freyer, J., Arnason, J., Eberl, G., Hamann, A., Wagner, H., Huehn, J., and Sparwasser, T. (2007). Selective depletion of FoxP3+ regulatory T cells induces a scurfy-like disease. J. Exp. Med. *204*, 57–63.

Lawson, V.J., Maurice, D., Silk, J.D., Cerundolo, V., and Weston, K. (2009). Aberrant selection and function of invariant NKT cells in the absence of AP-1 transcription factor Fra-2. J. Immunol. *183*, 2575–2584.

Lee, W., Kim, H.S., Baek, S.Y., and Lee, G.R. (2016). Transcription factor IRF8 controls Th1-like regulatory T-cell function. Cell. Mol. Immunol. *13*, 785–794.

Lee, W., Kim, H.S., Hwang, S.S., and Lee, G.R. (2017). The transcription factor Batf3 inhibits the differentiation of regulatory T cells in the periphery. Exp. Mol. Med. *49*, e393.

Liu, J.Z., van Sommeren, S., Huang, H., Ng, S.C., Alberts, R., Takahashi, A., Ripke, S., Lee, J.C., Jostins, L., Shah, T., et al.; International Multiple Sclerosis Genetics Consortium; International IBD Genetics Consortium (2015). Association analyses identify 38 susceptibility loci for inflammatory bowel disease and highlight shared genetic risk across populations. Nat. Genet. *47*, 979–986.

Lund, R.J., Löytömäki, M., Naumanen, T., Dixon, C., Chen, Z., Ahlfors, H., Tuomela, S., Tahvanainen, J., Scheinin, J., Henttinen, T., et al. (2007). Genome-wide identification of novel genes involved in early Th1 and Th2 cell differentiation. J. Immunol. *178*, 3648–3660.

Mantel, P.Y., Ouaked, N., Rückert, B., Karagiannidis, C., Welz, R., Blaser, K., and Schmidt-Weber, C.B. (2006). Molecular mechanisms underlying FOXP3 induction in human T cells. J. Immunol. *176*, 3593–3602.

Mathas, S., Kreher, S., Meaburn, K.J., Jöhrens, K., Lamprecht, B., Assaf, C., Sterry, W., Kadin, M.E., Daibata, M., Joos, S., et al. (2009). Gene deregulation and spatial genome reorganization near breakpoints prior to formation of translocations in anaplastic large cell lymphoma. Proc. Natl. Acad. Sci. U S A *106*, 5831–5836.

Mazur, E.C., Vasquez, Y.M., Li, X., Kommagani, R., Jiang, L., Chen, R., Lanz, R.B., Kovanci, E., Gibbons, W.E., and DeMayo, F.J. (2015). Progesterone receptor transcriptome and cistrome in decidualized human endometrial stromal cells. Endocrinology *156*, 2239–2253.

Miyazaki, M., Miyazaki, K., Chen, S., Itoi, M., Miller, M., Lu, L.F., Varki, N., Chang, A.N., Broide, D.H., and Murre, C. (2014). Id2 and Id3 maintain the regulatory T cell pool to suppress inflammatory disease. Nat. Immunol. *15*, 767–776.

Mootha, V.K., Lindgren, C.M., Eriksson, K.F., Subramanian, A., Sihag, S., Lehar, J., Puigserver, P., Carlsson, E., Ridderstråle, M., Laurila, E., et al. (2003). PGC-1alpha-responsive genes involved in oxidative phosphorylation are coordinately downregulated in human diabetes. Nat. Genet. *34*, 267–273.

Ochi, Y., Koizumi, T., Kobayashi, S., Phuchareon, J., Hatano, M., Takada, M., Tomita, Y., and Tokuhisa, T. (1994). Analysis of IL-2 gene regulation in c-fos transgenic mice. Evidence for an enhancement of IL-2 expression in splenic T cells stimulated via TCR/CD3 complex. J. Immunol. *153*, 3485–3490.

Ogawa, C., Tone, Y., Tsuda, M., Peter, C., Waldmann, H., and Tone, M. (2014). TGF-β-mediated FoxP3 gene expression is cooperatively regulated by Stat5, Creb, and AP-1 through CNS2. J. Immunol. *192*, 475–483.

Owen, D.L., Mahmud, S.A., Sjaastad, L.E., Williams, J.B., Spanier, J.A., Simeonov, D.R., Ruscher, R., Huang, W., Proekt, I., Miller, C.N., et al. (2019). Thymic regulatory T cells arise via two distinct developmental programs. Nat. Immunol. *20*, 195–205.

Povoleri, G.A.M., Nova-Lamperti, E., Scottà, C., Fanelli, G., Chen, Y.C., Becker, P.D., Boardman, D., Costantini, B., Romano, M., Pavlidis, P., et al. (2018). Human retinoic acid-regulated CD161^{+} regulatory T cells support wound repair in intestinal mucosa. Nat. Immunol. *19*, 1403–1414.

Schmiedel, B.J., Singh, D., Madrigal, A., Valdovino-Gonzalez, A.G., White, B.M., Zapardiel-Gonzalo, J., Ha, B., Altay, G., Greenbaum, J.A., McVicker, G., et al. (2018). Impact of genetic polymorphisms on human immune cell gene expression. Cell *175*, 1701–1715.e16.

Schneider, C.A., Rasband, W.S., and Eliceiri, K.W. (2012). NIH Image to ImageJ: 25 years of image analysis. Nature Methods *9*, 671–675.

Sekiya, T., Kashiwagi, I., Inoue, N., Morita, R., Hori, S., Waldmann, H., Rudensky, A.Y., Ichinose, H., Metzger, D., Chambon, P., and Yoshimura, A. (2011). The nuclear orphan receptor Nr4a2 induces FoxP3 and regulates differentiation of CD4+ T cells. Nat. Commun. *2*, 269.

Subramanian, A., Tamayo, P., Mootha, V.K., Mukherjee, S., Ebert, B.L., Gillette, M.A., Paulovich, A., Pomeroy, S.L., Golub, T.R., Lander, E.S., and Mesirov, J.P. (2005). Gene set enrichment analysis: a knowledge-based approach for interpreting genome-wide expression profiles. Proc. Natl. Acad. Sci. U S A *102*, 15545–15550.

Tan, H., Yang, K., Li, Y., Shaw, T.I., Wang, Y., Blanco, D.B., Wang, X., Cho, J.H., Wang, H., Rankin, S., et al. (2017). Integrative proteomics and phosphoproteomics profiling reveals dynamic signaling networks and bioenergetics pathways underlying T cell activation. Immunity *46*, 488–503.

Trapnell, C., Hendrickson, D.G., Sauvageau, M., Goff, L., Rinn, J.L., and Pachter, L. (2013). Differential analysis of gene regulation at transcript resolution with RNA-seq. Nat. Biotechnol. *31*, 46–53.

Trapnell, C., Williams, B.A., Pertea, G., Mortazavi, A., Kwan, G., van Baren, M.J., Salzberg, S.L., Wold, B.J., and Pachter, L. (2010). Transcript

assembly and quantification by RNA-Seq reveals unannotated transcripts and isoform switching during cell differentiation. Nat. Biotechnol. *28*, 511–515.

Tripathi, S.K., Chen, Z., Larjo, A., Kanduri, K., Nousiainen, K., Äijo, T., Ricaño-Ponce, I., Hrdlickova, B., Tuomela, S., Laajala, E., et al. (2017). Genome-wide analysis of STAT3-mediated transcription during early human Th17 cell differentiation. Cell Rep. *19*, 1888–1901.

Ubieta, K., Garcia, M., Grötsch, B., Uebe, S., Weber, G.F., Stein, M., Ekici, A., Schett, G., Mielenz, D., and Bozec, A. (2017). Fra-2 regulates B cell development by enhancing IRF4 and Foxo1 transcription. J. Exp. Med. *214*, 2059–2071.

Ye, B.D., and McGovern, D.P. (2016). Genetic variation in IBD: progress, clues to pathogenesis and possible clinical utility. Expert Rev. Clin. Immunol. *12*, 1091–1107.

STAR★METHODS

KEY RESOURCES TABLE

REAGENT or RESOURCE	SOURCE	IDENTIFIER
Antibodies		
CD3 (BV421, eFluor 450)	Biolegend/eBioscience	17A2; RRID: AB_2562553
CD4 (FITC, BV510)	Biolegend/eBioscience	RM4-5; RRID: AB_2561388
CD8 (BV711, APC)	Biolegend/eBioscience	53-6,7; RRID: AB_2535438
CD25 (APC)	eBioscience	PC61.5; RRID: AB_469366
CD44 (PE-Cy7)	eBioscience	IM7; RRID: AB_2535493
CD62L (PerCP-Cy5.5)	eBioscience	MEL-14; RRID: AB_996667
CD69 (PE)	eBioscience	H1.2F3; RRID: AB_2534935
CD45 (Pacific Blue)	Biolegend	30-F11; RRID: AB_493536
CD45.1 (APC-eFluor 780)	eBioscience	A20; RRID: AB_1582229
CD45.2 (Alexa Fluor 700)	eBioscience	104; RRID: AB_657753
Thy1.2 (eFluor450NC)	eBioscience	53-2.1; RRID: AB_1272237
FoxP3 (PE, Alexa Fluor 700)	eBioscience	FJK-16 s; RRID: AB_465936
F4/80 (PE)	Biolegend	BM8; RRID: AB_893486
CD19 (APC)	eBioscience	eBio1D3; RRID: AB_1659678
Ly6-G (PercP-eFluor 710)	eBioscience	1A8-Ly6g; RRID: AB_2573892
Ki67 (FITC)	eBioscience	SolA15; RRID: AB_11151330
IFNγ (APC)	eBioscience	XMG1.2; RRID: AB_469503
IL17A (PE-Cy7)	eBioscience	eBio17B7; RRID: AB_2534297
IL13 (PE-Cy7)	eBioscience	eBio13A; RRID: AB_2573529
IL5 (APC)	Biolegend	TRFK5; RRID: AB_315329
Deposited Data		
Raw and analyzed data	This paper	Gene Expression Omnibus: GSE132313
Experimental Models: Organisms/Strains		
Mouse: *Fosl2*^{tg}	In house	
Mouse: B6.Cg-Tg(Cd4-cre)1Cwi/BfluJ	The Jackson Laboratory	Jax: 022071
Mouse: B6(Cg)-*Rag2*$^{tm1.1Cgn}$/J	The Jackson Laboratory	Jax: 008449
Mouse: Fosl2^{tm2Wag}	Pr Bozec Erlangen	N/A
Mouse: CByJ.SJL(B6)-*Ptprc*^{a}/J	The Jackson Laboratory	Jax: 006584
Oligonucleotides		
Fosl2^{tg} mice Forward: GCACGACTTCTTCAAGTCCGCCATGCC	This paper	N/A
Fosl2^{tg} mice Reverse: GCGGATCTTGAAGTTCACCTTGATGCC	This paper	N/A
Fosl2^{fl} Forward: GAGGGAGTTGGGGATAGAGTGGTA	This paper	N/A
Fosl2^{fl} Reverse: GGACAGCAGGTCAGGAGTAGATGA	This paper	N/A
CD4-cre Forward: CCCAACCAACAAGAGCTCAAG	This paper	N/A
CD4-cre Reverse: CCCAGAAATGCCAGATTACG	This paper	N/A
Software and Algorithms		
ImageJ	Schneider et al., 2012	https://imagej.nih.gov/ij/

RESOURCE AVAILABILITY

Lead Contact

Requests concerning further information and resources, or reagents should be made to the lead contact, Oliver Distler (oliver.distler@usz.ch)

Materials Availability

Fosl2^{tg} mice are available through MTA as rights belongs to Sanofi.

This study did not generate new unique reagents.

Data and Code Availability

Data from our RNA seq experiment have been deposited in the GEO database: RNA-seq data accession code: Gene Expression Omnibus: GSE132313.

EXPERIMENTAL MODEL AND SUBJECT DETAILS

Animals

C57Bl6 and *Rag2*$^{-/-}$ mice were purchased from Jackson Laboratory. *Fosl2*$^{fl/fl}$ mice were obtained from Aline Bozec (University of Erlangen) and rederivated by embryo transfer, CD4-cre and FoxP3-GFP mice were obtained from Burkhard Becher (University of Zurich), Ly5.1 mice were obtained from Onur Boyman (University Hospital Zurich). All mice were housed in pathogen free conditions. We received approval for all animal experiments from the Cantonal Veterinary Office Zurich.

Fosl2^{tg} mice were generated by Arun Subramaniam (Sanofi-Genzyme). A vector containing the murine *Fosl2* gene (Exons 1 to 4, corresponding introns, and truncated UTRs) under the control of the MHCI promotor H2Kb was randomly inserted into the genome (Figure S1A). The eGFP sequence was inserted in frame after the Fosl2 transgene as a marker. To avoid generation of a Fosl2-eGFP fusion protein, a self-cleaving peptide T2A (Thosea asigna virus 2A) was inserted between the two coding sequences, creating a bi-cistronic transgene. The 2A self-cleaving peptide induces cleavage of the amino-acid chain during translation, giving rise to two separate proteins without the need of adding an IRES sequence.

We used the following primers for genotyping:

Fosl2^{tg} mice Forward: "GCACGACTTCTTCAAGTCCGCCATGCC"
Fosl2^{tg} mice Reverse: "GCGGATCTTGAAGTTCACCTTGATGCC"
Fosl2^{fl} Forward: "GAGGGAGTTGGGGATAGAGTGGTA"
Fosl2^{fl} Reverse: "GGACAGCAGGTCAGGAGTAGATGA"
CD4-cre Forward: "CCCAACCAACAAGAGCTCAAG"
CD4-cre Reverse: "CCCAGAAATGCCAGATTACG"

The *Rag2*$^{-/-}$ mice genotype was confirmed by flow cytometry staining of T cells in blood samples. *Fosl2*^{tg} were also phenotyped by analyzing GFP expression in peripheral blood mononuclear cells (PMBCs) by flow cytometry.

Age of the mice used in the different experiments is indicated in the Figure legends. Whenever an experiment was performed using only males or females, this is also mentioned in figure legends or the method section. All mice in this study have been backcrossed for more that 10 generation on a C57Bl6/J background. Mice were housed in pathogen free conditions.

METHOD DETAILS

Experimental Autoimmune Encephalomyelitis

Age- and sex-matched 6-12 week old mice were used for all experiments. Mice were immunized with 200μg MOG_{35-55} emulsified in CFA and treated with 200ng Pertussis toxin (i.p.) on the day of immunization and again two days later. Mice were monitored for weight loss and scored by a blinded experimenter for clinical symptoms for 15 days.

Flow cytometry

For all flow cytometry and cell sorting experiments, we used PBS with 1% FCS and 1mM EDTA (FACS buffer). Spleen and lymph nodes were gently smashed through a 70 μm cell strainer. Cells were washed once in FACS buffer and red blood cells were lysed using RBC lysis buffer (Biolegend).

The following antibodies were used for flow cytometry and cell sorting (dilutions 1:100 to 1:400). From eBioscience, Biolegend or BD: CD25 (clone PC61.5), CD44 (clone IM7), CD62L (clone MEL-14), CD69 (clone H1.2F3), CD45.1 (APC-eFluor 780, clone A20), CD45.2 (clone 104), Thy1.2 (clone 53-2,1), FoxP3 (clone FJK-16 s), Ki67 (clone SolA15), CD3 (clone 17A2), CD4 (clone GK1.5 or RM4-5), CD8 (clone 53-6, 7), Helios (clone 22F6), Neuropillin1 (clone 3E12), CD19 (clone 1D3 or 6D5), CD45 (clone 30-F11),

CTLA4 (clone UC10-F10), CD40L (clone MR1), GITR (clone DTA-1), CD27 (clone LG.3A10), TIGIT (clone I1G9), PD-1 (clone 29F.1A12). For staining of FoxP3, we used the FoxP3 staining buffer set (eBioscience).

Exclusion of dead cell was based on Fixable viability dye eFluor 780 (eBioscience) Zombie Yellow (Biolegend) or Propidium Iodide (eBioscience). For compensation, we used cells or UltraComp eBeads (Invitrogen) and compensation was calculated at the time of acquisition on the BD FACSDiva software. For cell quantification, we used Precision Count Beads (Biolegend).

All samples were acquired on the BD LSRFortessa II or FACSymphony flow cytometer using BD FACSDiva software. Cell sorting was done on BD FACSAria III cell sorter. Data analysis was performed on FlowJo 10.0.8r1. Example of gating strategy is shown in Figure S4.

Histology and Immunohistochemistry

For histology, we perfused the circulatory system immediately after euthanasia by opening the right atria and slowly injecting 10ml of PBS in the right ventricle using a 24G needle. Entire organs were then collected, washed in PBS and fixed for 16 h in 4% paraformaldehyde in PBS. Tissues were then washed in distilled water and transferred to 50% ethanol. Organs were dehydrated by 3 one h incubations in 80% ethanol, followed by 3 one h incubations in 96% ethanol, followed by 2 one h incubations in 100% ethanol. Tissues were then cleared twice in xylene for one h and subsequently kept in a 56°C paraffin bath, twice, for 3 h. After paraffin embedding, 4 μm thick sections were placed on Superfrost Plus slides (Thermo Scientific) and dried overnight.

For all subsequent stainings, sections were de-paraffinised by washing three times in xylene for 10 min and rehydrated by sequential incubations in 100%, 100%, 96% and 80% ethanol solutions for 3 min each. Sections were finally incubated for 5 min in distilled water.

For H&E staining, rehydrated sections were incubated for 10 min in Mayer's hematoxylin solution (J.T Baker) and rinsed for 10 min in running tap water. Sections were stained for one min in eosin 1% solution (Reactolab) and quickly rinsed in distilled water before dehydration with increasing ethanol concentration.

For immunohistochemistry, antigen retrieval was performed on rehydrated sections. In brief, sections were boiled in citrate buffer (10mM Citrate, 0.05% tween, pH = 6) with a microwave, and further incubated at 95°C in an oven for 15 min. Sections were left to cool down and washed in PBS. To block endogenous peroxidases, sections were incubated 15 min in 3% H_2O_2 solution and rinsed twice in PBS-Tween for 5 min. To block unspecific antibody binding, sections were incubated for one h in blocking solution (10% goat serum in Background Reducing Antibody Diluent from Dako). Endogenous biotin was blocked using the Avidin-Biotin Block kit (from Vector Laboratories). The primary antibody was incubated overnight at 4°C followed by two washings in PBS-Tween for 5 min. The biotinylated secondary antibody was incubated for 30 min at room temperature. After washing twice with PBS-Tween for 5 min, sections were incubated for 30 min with VECTASTAIN Elite ABC solution (Vector Laboratories) and washed twice in PBS for 5 min. Staining was developed using DAB (from Vector Laboratories) followed by a counterstaining of nuclei for 1 min in Mayer's hematoxylin solution (J.T Baker). All stainings were mounted using Pertex mounting medium.

Cell culture

We used DMEM containing high glucose (4.5 g/l), 10% heat inactivated FCS, pyruvate (0.11 g/l), L-Glutamate (0.58 g/l) supplemented with MEM Vitamins solution (GIBCO), MEM Non-essential amino acids (GIBCO) and β-mercaptoethanol (50mM).

RT-qPCR

RNA was extracted from cell pellets using Quick RNA MicroPrep /Zymo Research). RNA was quantified using the Nano-drop ND1000 (Thermo Fisher). Two hundred ng of RNA was then reverse transcribed using the transcriptor First Strand cDNA synthesis kit (Roche) with oligo-dT primers. qPCR was performed using SYBR green GoTaq qPCR master mix (Promega) on Agilent Startagen Mx3005P qPCR system. Relative expression was calculated using the ΔΔCt method.

Western-blot

For cell lysis, we used RIPA buffer (Sigma-Aldrich) supplemented with protease and phosphatase inhibitor tablets (EASYpack Protease inhibitor cocktail, PhosphoSTOP both from Sigma-Aldrich), sample reducing agent (Life Technologies) and Pierce universal nuclease for DNA digestion (Thermo Scientific). Cells were lysed at 20 million cells per ml of lysis buffer; mixed with 4x LDS loading buffer (Life Technologies) and boiled at 95°C for 5 min. Electrophoresis and wet transfer were made using the Mini Protean system from BioRad. Lysates were separated with a 12% SDS-PAGE and transferred on nitrocellulose membranes. Membranes were blocked for 1 h with 5% milk proteins in TBS-Tween before incubation with the primary antibody overnight at 4°C. HRP conjugated secondary antibodies were incubated for 45 min at room temperature (1:10000 Jackson Immunolabs). We used SuperSignal West Pico Chemiluminescent Substrate (Thermo Scientific) for development on the Fusion Fx (Vilber). For protein size assessment, we used the PageRuler Plus protein ladder (Thermo Scientific). We screened available anti-Fosl2 antibodies using our *Fosl2*^{tg} and *Fosl2*$^{-/-}$ cells to validate specificity. The monoclonal antibody REY146C (1:1000) from Merk Millipore was selected as it showed increased signal in overexpressing cells and no signal was detected in ko cells (Figure S1D). Other antibodies were from Cell Signaling and were used at 1:1000: phosphor-c-Fos (clone D82C12), total c-Fos (clone 9F6), c-Jun (clone 60A8) and GAPDH (clone 14C10).

ELISA and multiplex

For quantification of immunoglobulins, cytokines, and chemokines, we collected blood from the vena cava immediately after euthanasia of wt or *Fosl2*^{tg} mice. Serum was collected after spin down of the blood and snap frozen for later analysis. Cytokines, chemo-

kines and immunoglobulines levels in the serum of wt and *Fosl2*^{tg} mice (17 weeks old, males and females) were measured using a 25 parameter multiplex assay or individual ELISA.

Cytokines and chemokines analyzed included G-CSF, GM-CSF, IFN-γ, IL-1α, IL-1β, IL-2, IL-4, IL-5, IL-6, IL-7, IL-9, IL-10, IL-12 (p40), IL-12 (p70), IL-13, IL-15, IL-17, IP-10, KC, MCP-1, MIP-1α, MIP-1β, MIP-2, RANTES, TNF-α (Millipore MAP mouse cytokine/chemokine magnetic kit, cat# MCYTOMAG 70k PMX). The assay was performed in 96 well plates in duplicates following manufacturer's protocol and data acquired on a Milliplex analyzer (Luminex SD). IgG and IgE levels were quantified in the serum of 16 week old females using Ready-SET go Elisa kit for mouse from eBioscience. The assay was performed in duplicates.

RNA-sequencing

Total RNA was isolated from the samples using QIAGEN's RNeasy Mini Kit. RNA integrity number values ranged from 8.1 to 10.0. Directional Poly-A RNA-seq libraries were prepared and sequenced as PE42 (42-bp paired-end reads) on Illumina NextSeq 500 to a depth of 35-64M read pairs. The "TopHat" algorithm was used to align the reads to the mm10 genome. The alignments (32-60M aligned pairs) in the BAM files were further analyzed using the Cufflinks suite of programs (running consecutively: Cufflinks → Cuffcompare → Cuffdiff) (Trapnell et al., 2010, Trapnell et al., 2013). Cufflinks was run using the mm10-genes as a reference database. By doing so, the output shows the known genes with their RNA-Seq metrics (as FPKM = Fragments Per Kilobase of exon model per Million mapped fragments), but novel transcripts are not identified. The 9 (3 × 3 replicates) cufflinks outputs were compared using cuffdiff.

We obtained a total of 2679 genes for control versus *Fosl2*^{tg}, 1150 genes for control versus *Fosl2*$^{-/-}$ and 3510 genes for *Fosl2*^{tg} versus *Fosl2*$^{-/-}$. In total, there were 4123 genes differentially regulated in a least one of the pairwise comparisons.

We then filtered genes with a fold change >1.5, and with consistent (opposite) change between *Fosl2*^{tg} and *Fosl2*$^{-/-}$ cells. We thus selected the genes, which showed an upregulation in *Fosl2*^{tg} and a downregulation in *Fosl2*$^{-/-}$ and the genes showing a downregulation in *Fosl2*^{tg} and an upregulation in *Fosl2*$^{-/-}$. For enrichment analysis, we used the Gene Set Enrichment Analysis software.

Imaging and immunohistochemistry quantification

Images were acquired on an Olympus BX53 microscope with a DP80 camera.

For relative quantification of immunohistochemistry signals, we scanned the entire slide to avoid potential bias in selecting a region of interest for the analysis. DAB (brown) and hematoxylin (nuclei signal, blue) signals were separated using the Color Deconvolution plugin of ImageJ. One threshold was applied to all images on brown signal to obtain the number of DAB positive pixels and a second one was applied to the blue signal to obtain number of nuclei pixels. We then used the ratio DAB/hematoxylin to compare conditions.

T cell transfer

We used 3-5 week old *Fosl2*^{tg} mice as donors of T cells before the onset of autoimmunity. We used age and sex matched C57Bl6 mice as donors of CD45.2 wt cells, and Ly5.1 mice as donors of CD45.1 wt cells.

Spleens and LN CD4^{+} T cells were purified by magnetic separation using the CD4 T cell negative isolation kit (Miltenyi Biotec). Purity was assessed by flow cytometry and was routinely >95%–98%. Tregs were sorted as CD4^{+}CD25^{+} to a purity of >98%. More than 95% of these cells were FoxP3^{+} in subsequent analysis. 6-12 week old sex matched *Rag2*$^{-/-}$ recipients received the indicated cell numbers by i.v injection in a volume of 200 μL.

Bone marrow transfer

Bone marrow was extracted from the femurs and tibias of 6-8 week old donor mice by flushing the bones with PBS using a 24G needle. Red blood cells were lysed using RBC lysis buffer (Biolegend). T cells were depleted using biotinylated anti-CD3 antibody coupled to avidin magnetic beads (Miltenyi Biotec). 6-12 week old *Rag2*$^{-/-}$ sex-matched mice were used as recipients. One week prior to the experiment, recipient mice were treated with antibiotics in drinking water: Sulfodoxinum (1.33 mg/ml final concentration) and Trimethoprimum (0.26 mg/mL final concentration). They then received a 500 rad irradiation split in 2 doses, 4 h apart, 24 h before transfer of the bone marrow. Each recipient received 5*10^{6} bone marrow cells by intravenous injection in the tail in a volume of 200 μL. Antibiotic treatment was continued for one week after bone marrow reconstitution.

Treg suppression assay

For the *in vitro* Treg suppression assay, we sorted CD4^{+}CD25^{+}CD62L^{low}CD44^{high} cells as Tregs and CD4^{+}CD25^{-} cell as responders (Tresp). We used CD4^{-} splenocytes as antigen presenting cells (APC). To avoid proliferation of APCs, we treated them for 3 h with 50 μg/mL mytomycin C (Sigma-Aldrich), in medium at 37°C, followed by extensive washing to remove residual mytomycin C. To follow the proliferation of Tresp, we stained them with Cell Trace Violet (Invitrogen) prior to the assay. In round bottom 96 well plates, we seeded 200 000 APCs with 40 000 Tresps. Cells were stimulated with soluble anti-CD3 at a final concentration of 1 μg/ml. Tregs were added at the following Tresp/Treg ratios: 1:0, 1:1, 2:1, 4:1 and 8:1. After four days, we used propidium iodide to exclude dead cells and proliferation of live Tresp was measured by analysis of the number of cell divisions within the Cell Trace Violet^{+} Tresp cells.

T cell polarizing conditions

For *in vitro* T cell polarization, naive $CD4^{+}CD62L^{high}CD44^{low}$ cells were sorted. Ninety-six or 24 well plates were coated with anti-CD3 antibodies (2 μg/ml) for 2 h at 37°C and washed. We used anti-CD28 as co-stimulation (2 μg/ml). Polarization was induced as follows: Th1 mIL-12 (20 ng/ml) anti-IL-4 (1 μg/ml); Th2 mIL-4 (20 ng/ml) anti-IFNγ (1 μg/ml); Th17 mIL-6 (60 ng/ml) hTGFβ (1 ng/ml) anti-IL-4 (1 μg/ml) anti-IFNγ (1 μg/ml); iTreg: hTGFβ (10 ng/ml) anti-IL-4 (1 μg/ml) anti-IFNγ (1 μg/ml). After three days of stimulation, CD3/CD28 stimulation was stopped and cells were transferred to new wells with the same polarization conditions. Two days later, polarization was assessed by analysis of cytokine production and expression of FoxP3 as described in the flow cytometry section.

QUANTIFICATION AND STATISTICAL ANALYSIS

All statistical analyses were done using GraphPad Prism 8.0.0. As sample size in certain experiments was limited to determine normal distribution and since our size effect and statistical power was not a limitation we used non parametric tests, and plotted the median. The statistic test used and number of biological replicates is detailed in the legend of each figure. We also used dot plots to display individual values to better represent data distribution.